

Preformed magnetic clusters in the paramagnetic phase of a high-temperature ferromagnetic metal-organic framework

Giacomo Prando

Dipartimento di Fisica “Alessandro Volta”, Università di Pavia, Italy

B. Costarella, A. Apaix – ENS, France and Università di Pavia, Italy

C. Aloisi, M. C. Mozzati, P. Carretta – Università di Pavia, Italy

G. Allodi – Università di Parma, Italy

G. Lamura – CNR and Università di Genova, Italy

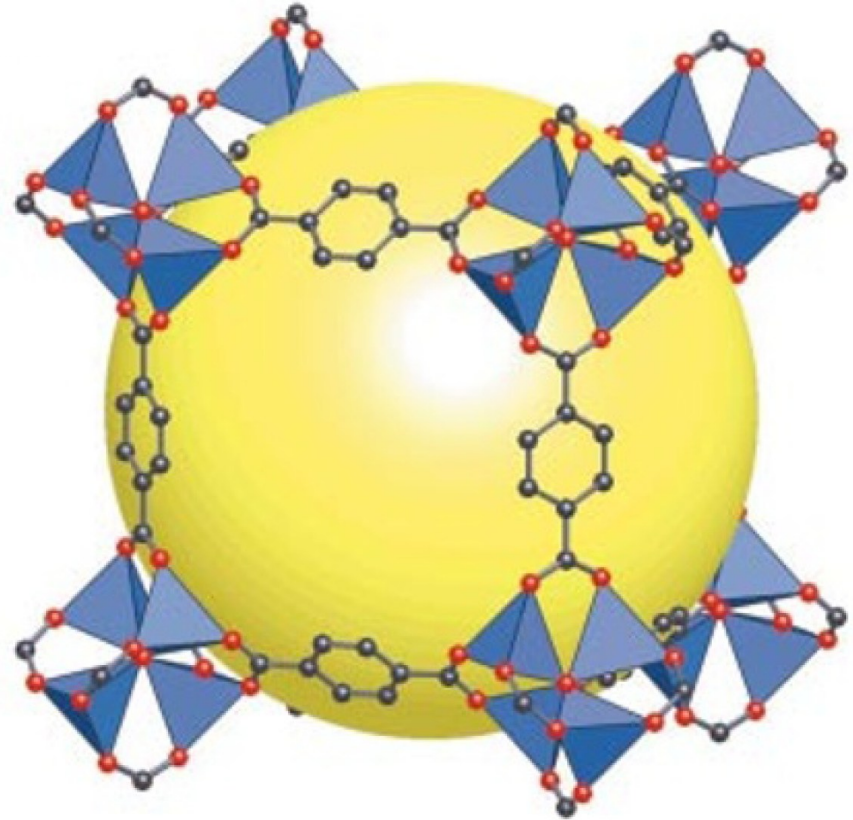
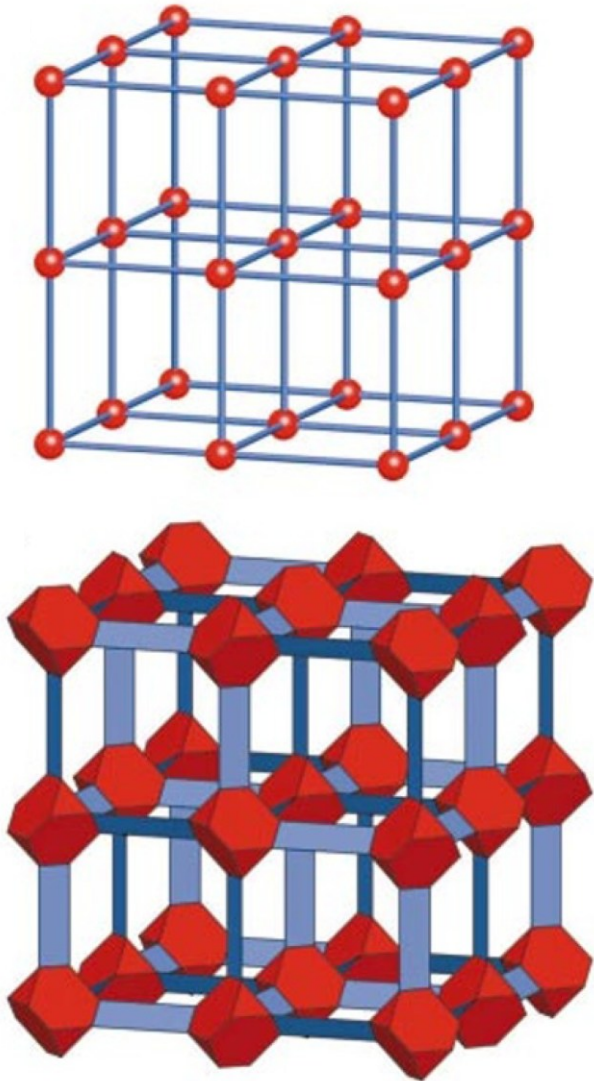
M. Dickson, J. G. Park, R. A. Murphy, T. D. Harris, J. R. Long – University of California, Berkeley

25.07.2025

MuSR 2025, Saint John's

Metal-organic frameworks (MOFs)

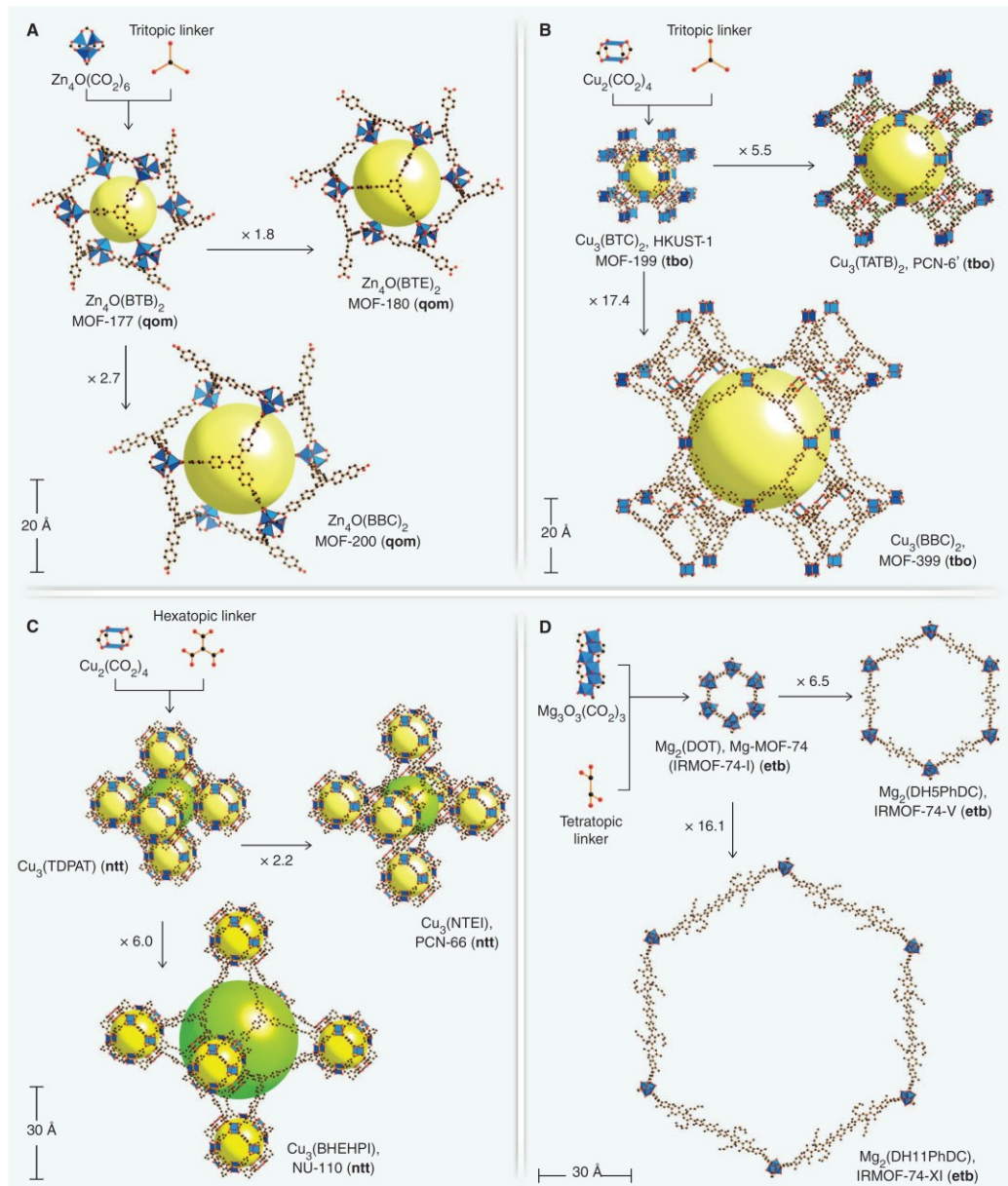
Coordination solids / coordination polymers.



“MOF-5”

- Inorganic ZnO_4 tetrahedra (vertices).
- Organic benzene dicarboxylate (“bonds”).
- Yellow sphere: 12 Å diameter.

Metal-organic frameworks (MOFs)



Exceptional tunability of the chemical/structural properties.

Very high porosity and surface/volume ratios. Relevant for:

- catalysis;

- gas adsorption, storage and separation.

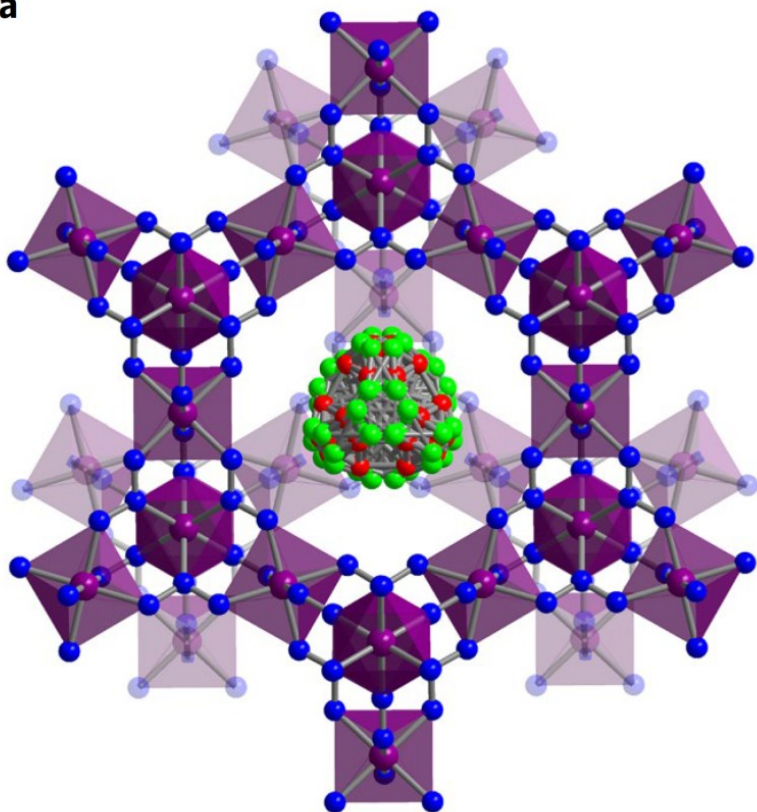
Chemical flexibility: tailored, “ad-hoc” electronic properties.

Magnetic/multiferroic MOFs: low T_c (weak exchange couplings).

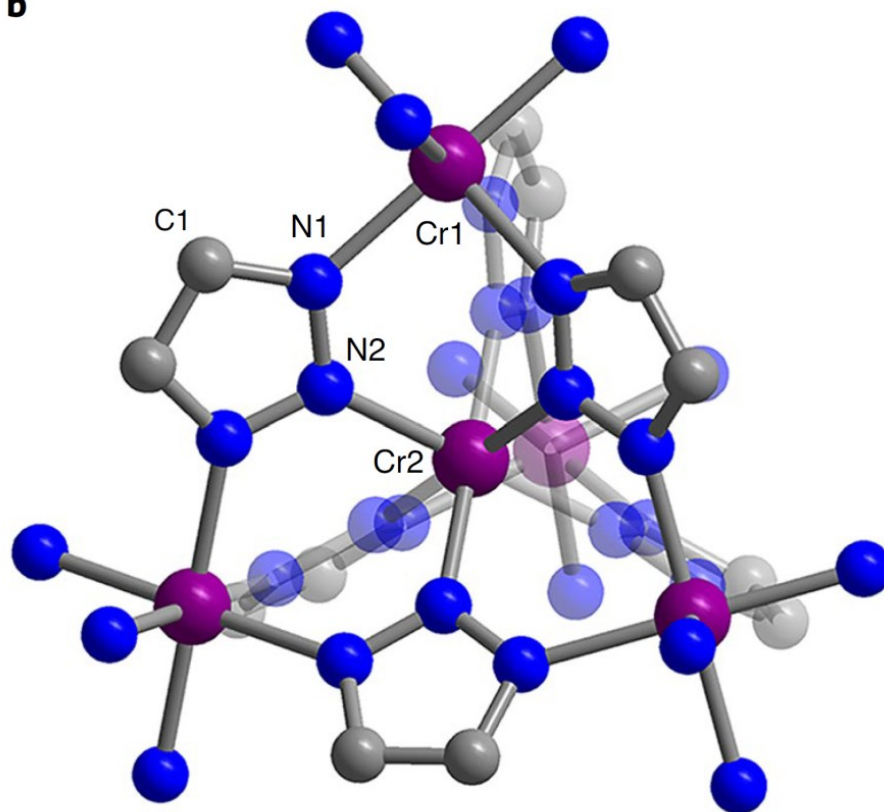
High-temperature ferromagnetism



a

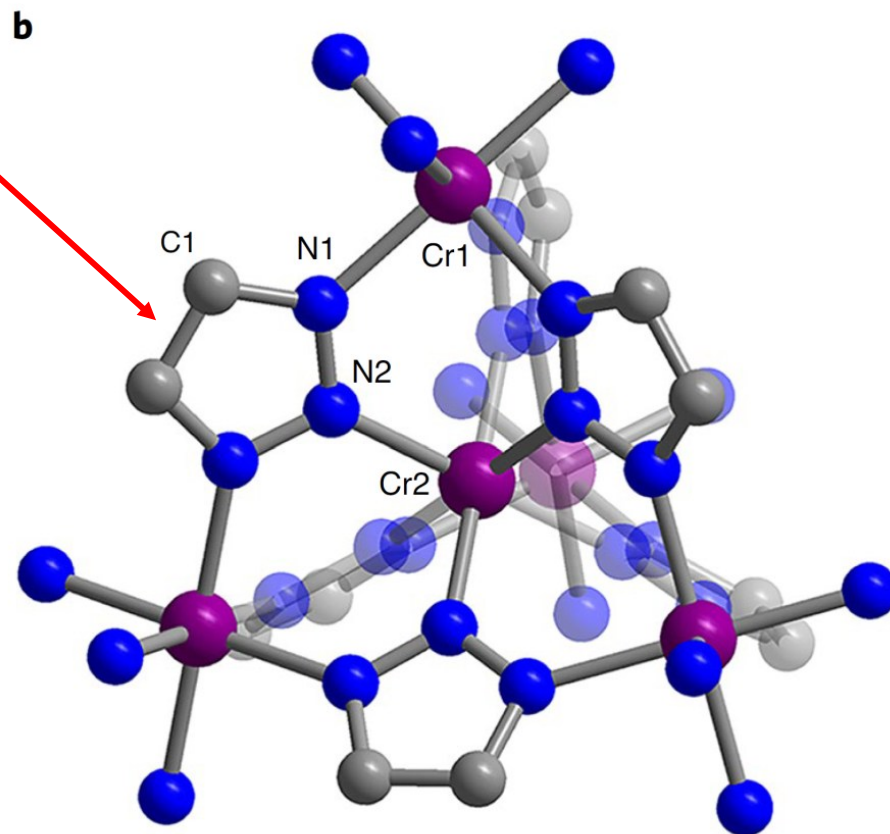
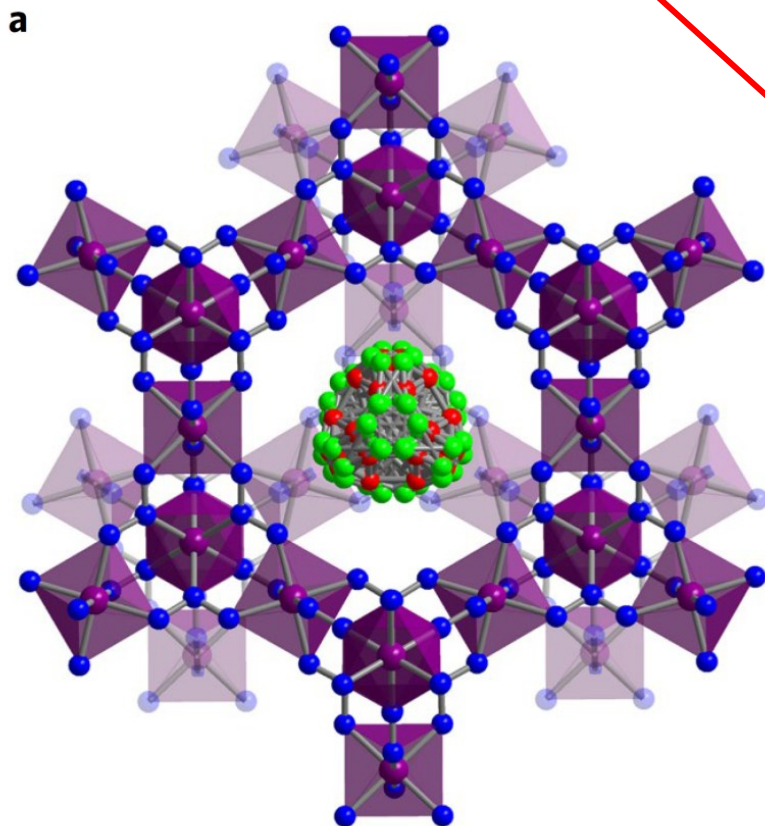


b



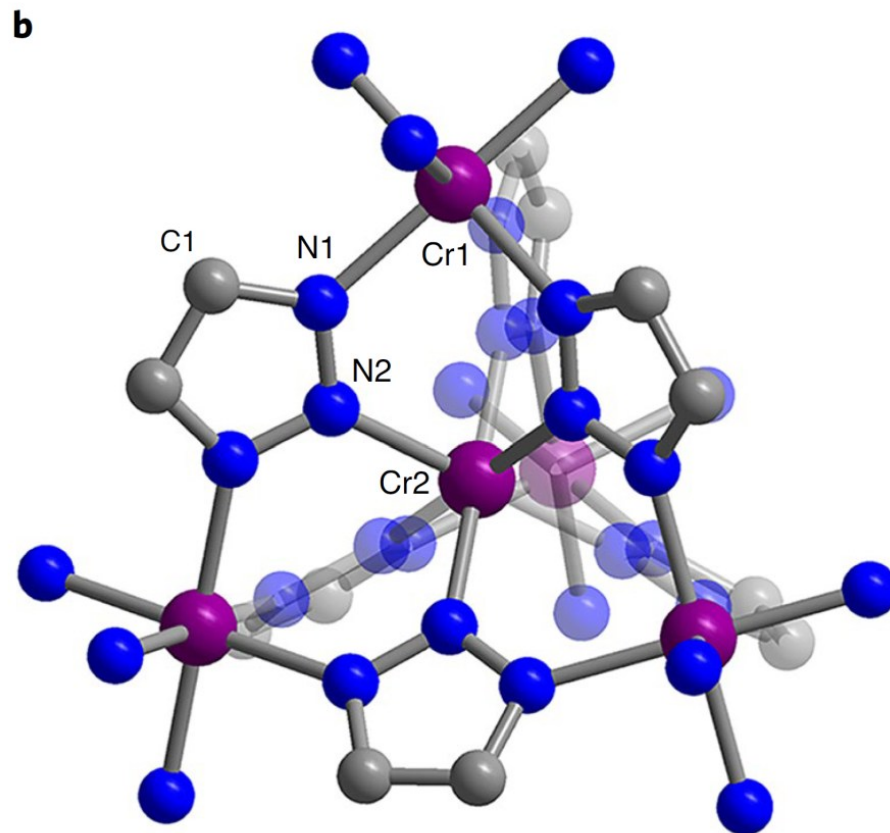
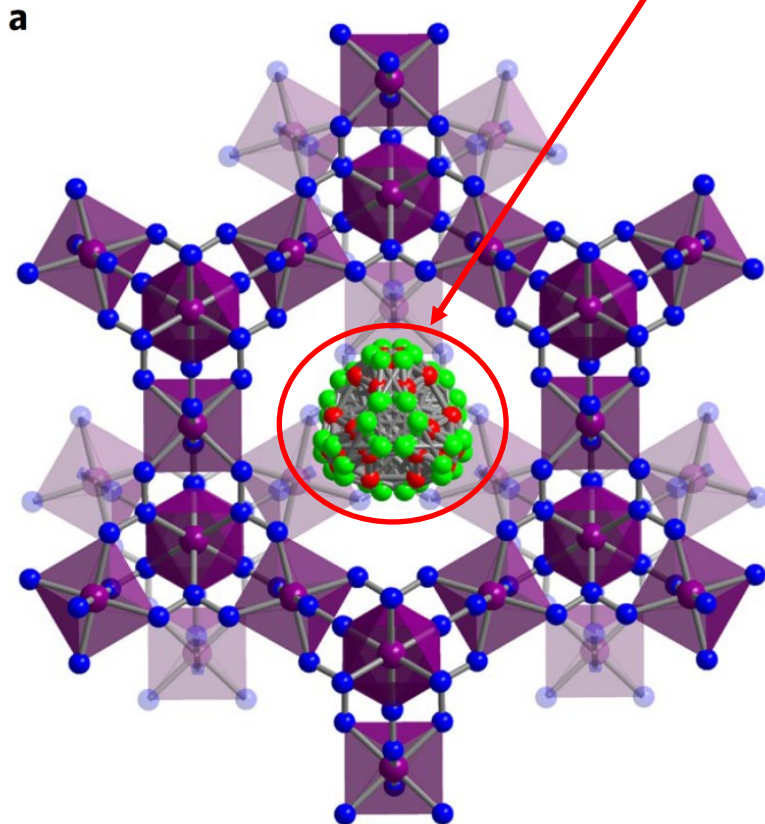
Triflate (CF_3SO_3)⁻ anion: mixed valence $\text{Cr}^{2+}/\text{Cr}^{3+}$.

High-temperature ferromagnetism



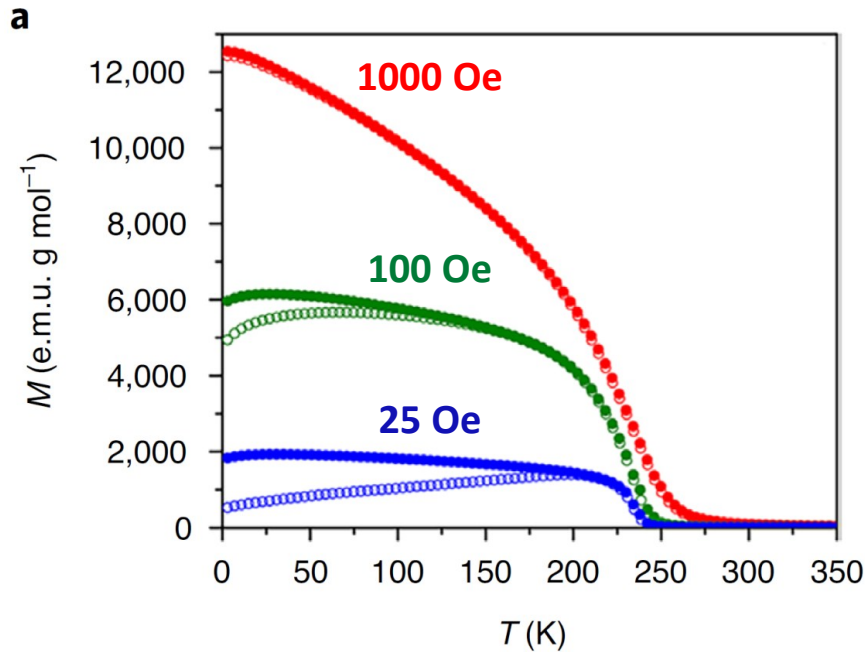
Triflate $(\text{CF}_3\text{SO}_3)^-$ anion: mixed valence $\text{Cr}^{2+}/\text{Cr}^{3+}$.

High-temperature ferromagnetism



Triflate $(\text{CF}_3\text{SO}_3)^-$ anion: mixed valence $\text{Cr}^{2+}/\text{Cr}^{3+}$.

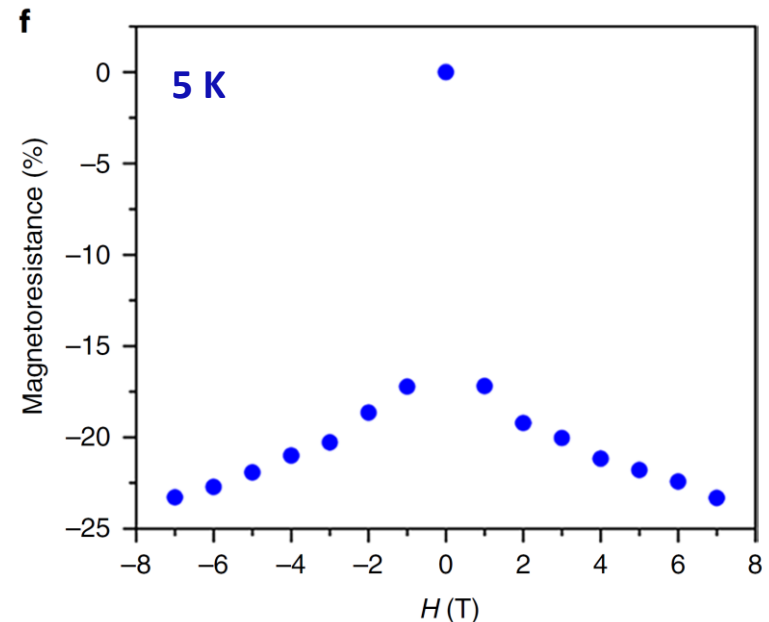
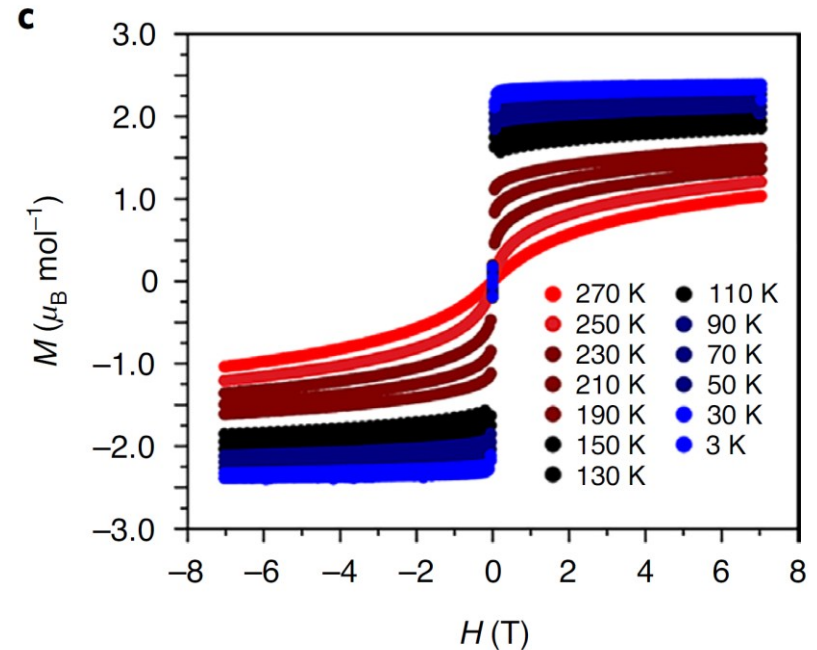
High-temperature ferromagnetism



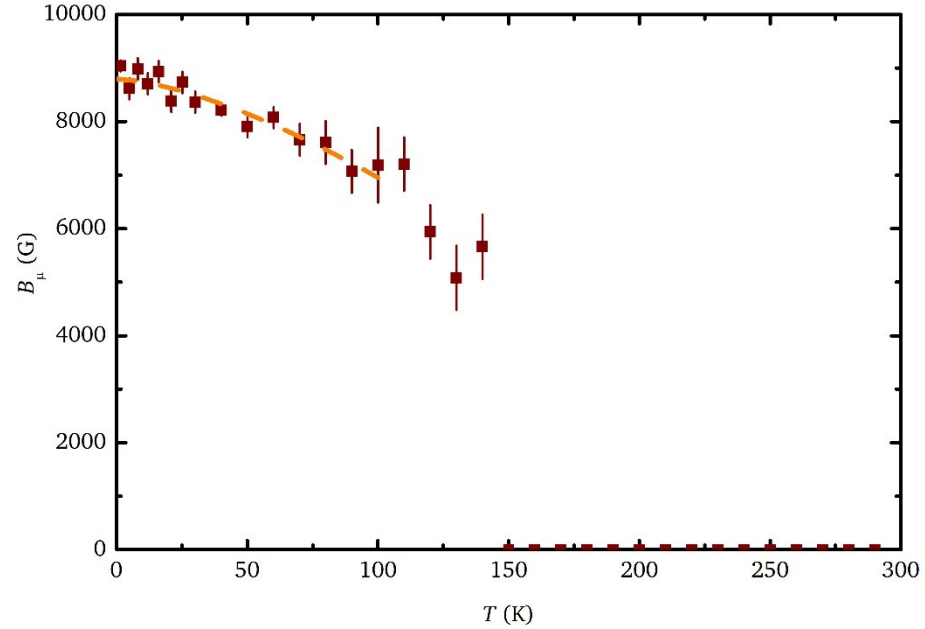
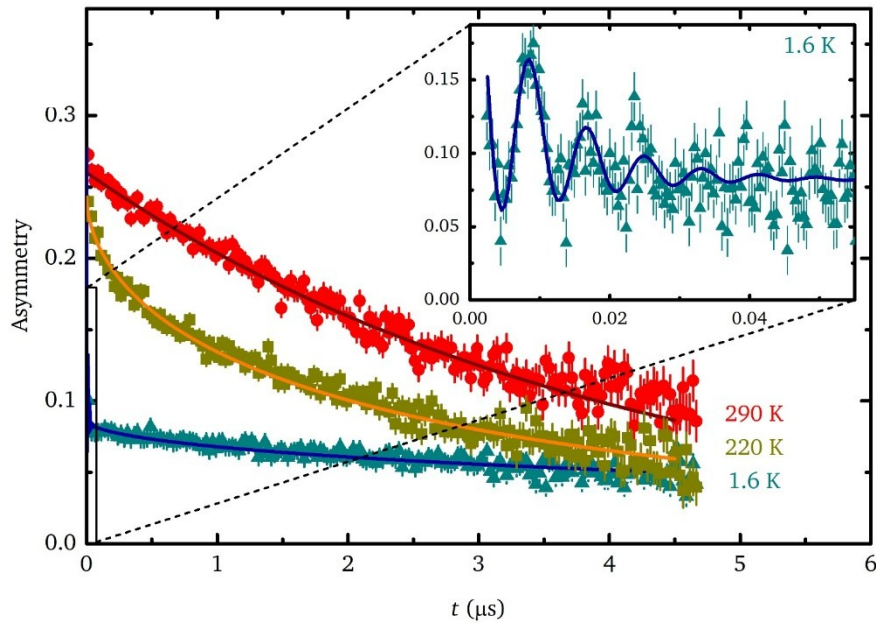
Highest critical temperature for MOFs
(around 225 K).

Among highest values
of magnetoresistance for MOFs.

Itinerant ferromagnetism arising from
double-exchange (Cr mixed valence).



Muon-spin rotation

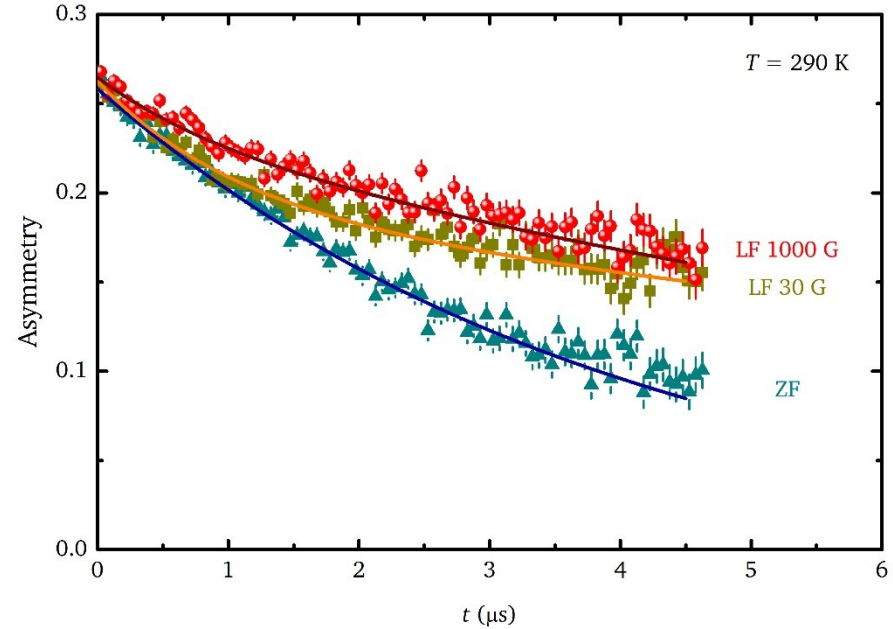
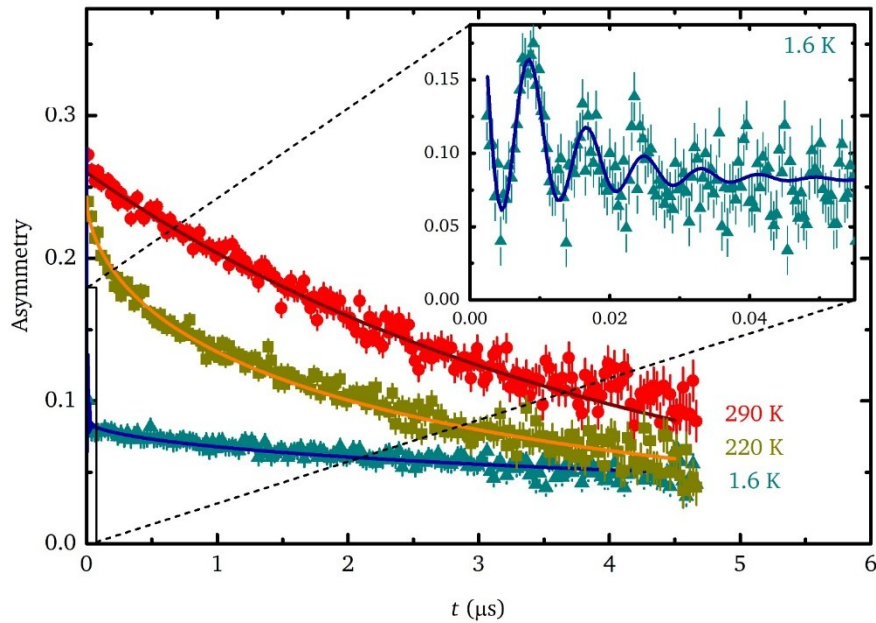


$$\frac{A(t)}{A(0)} = a_{T_1} \cos(\gamma_\mu B_\mu t + \phi) \exp(-\lambda_{T_1} t) + a_{T_2} \exp(-\lambda_{T_2} t) + a_L \exp(-\lambda_L t)$$

Likely implantation site close to Cr ions.

Low-temperatures Bloch-like $T^{3/2}$ law (FM).

Muon-spin rotation



$$\frac{A(t)}{A(0)} = a_{T_1} \cos(\gamma_\mu B_\mu t + \phi) \exp(-\lambda_{T_1} t) + a_{T_2} \exp(-\lambda_{T_2} t) + a_L \exp(-\lambda_L t)$$

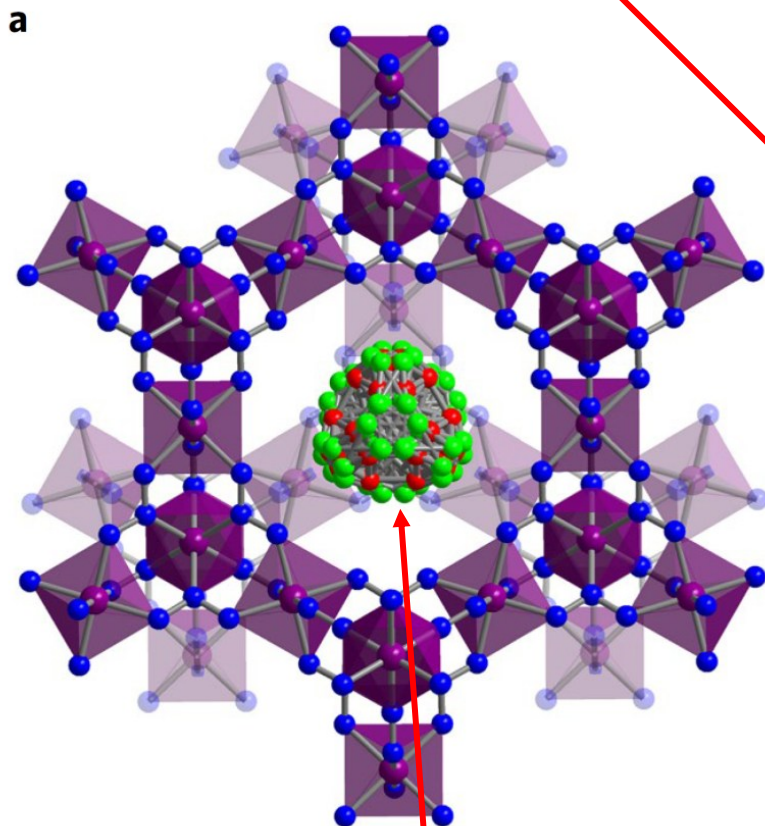
Likely implantation site close to Cr ions.

Low-temperatures Bloch-like $T^{3/2}$ law (FM).

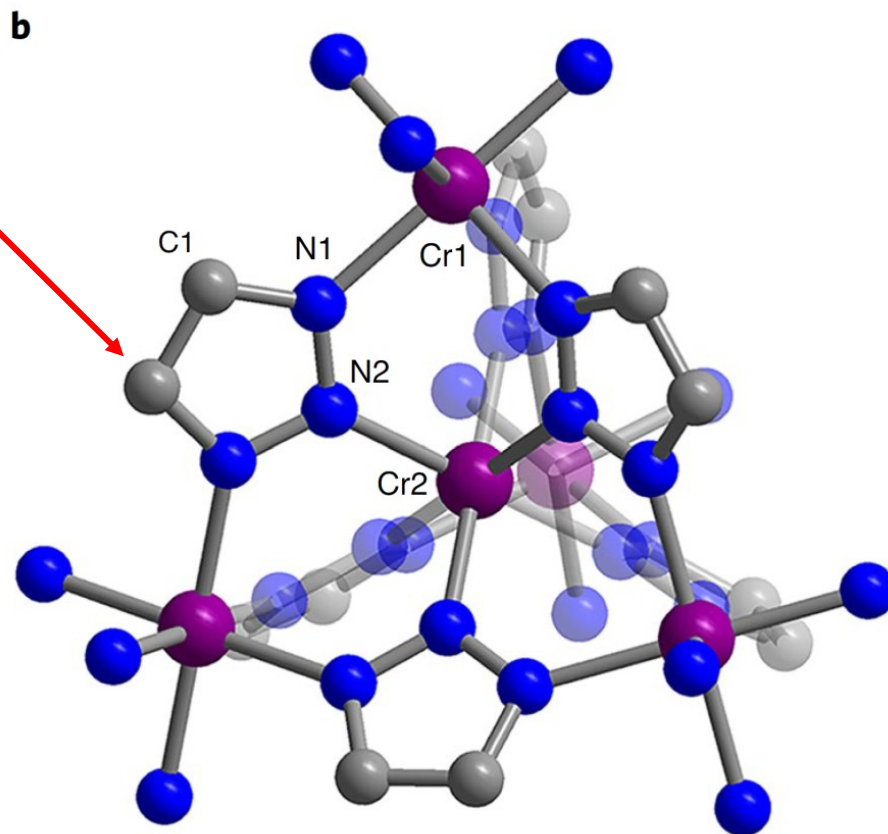
Unusual survival of dynamics well-above the critical temperature.

Nuclear magnetic resonance

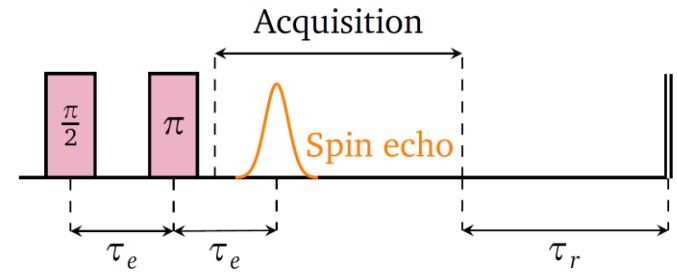
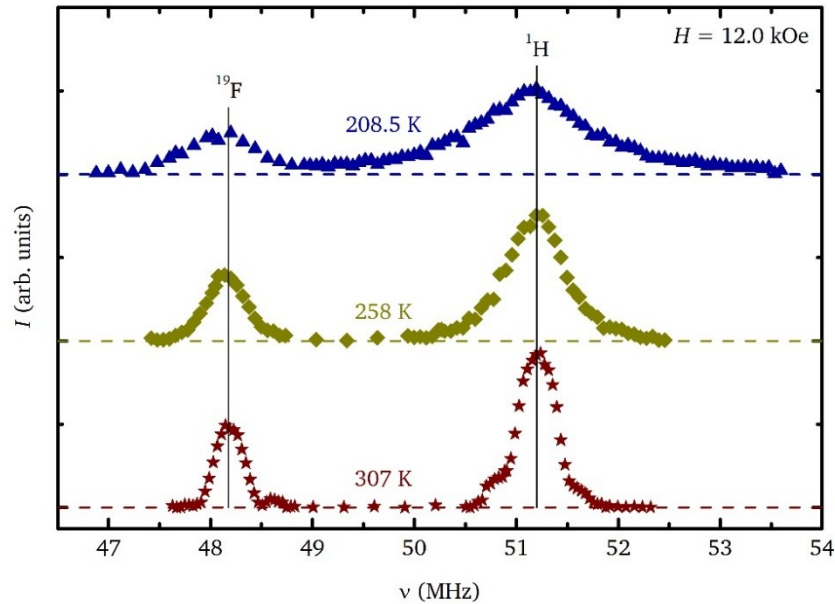
^1H nuclei in the metal-organic framework.



^{19}F nuclei in the charge-balancing triflate anion.

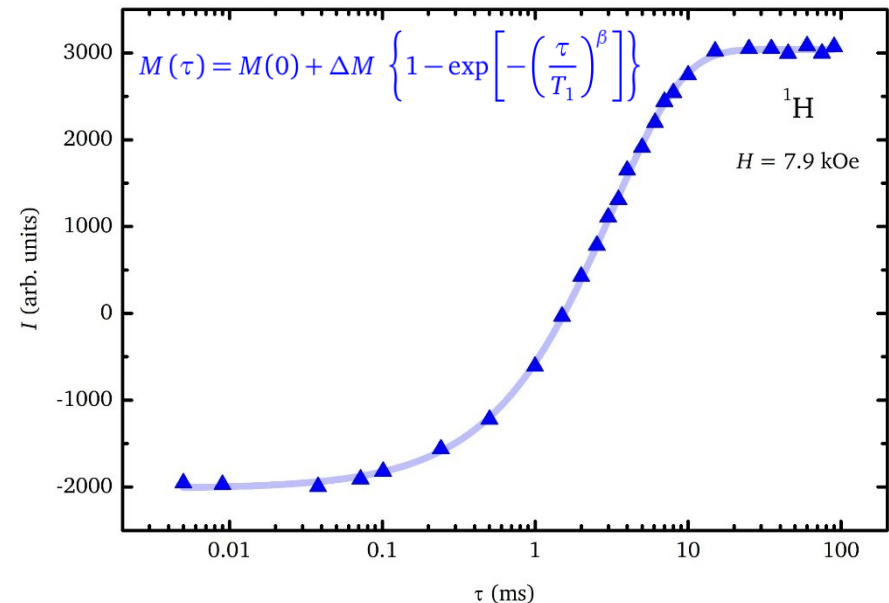
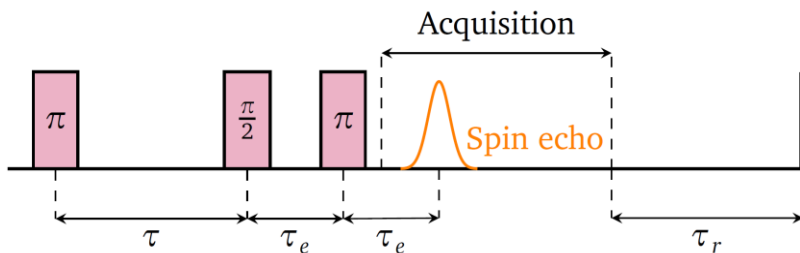


Nuclear magnetic resonance



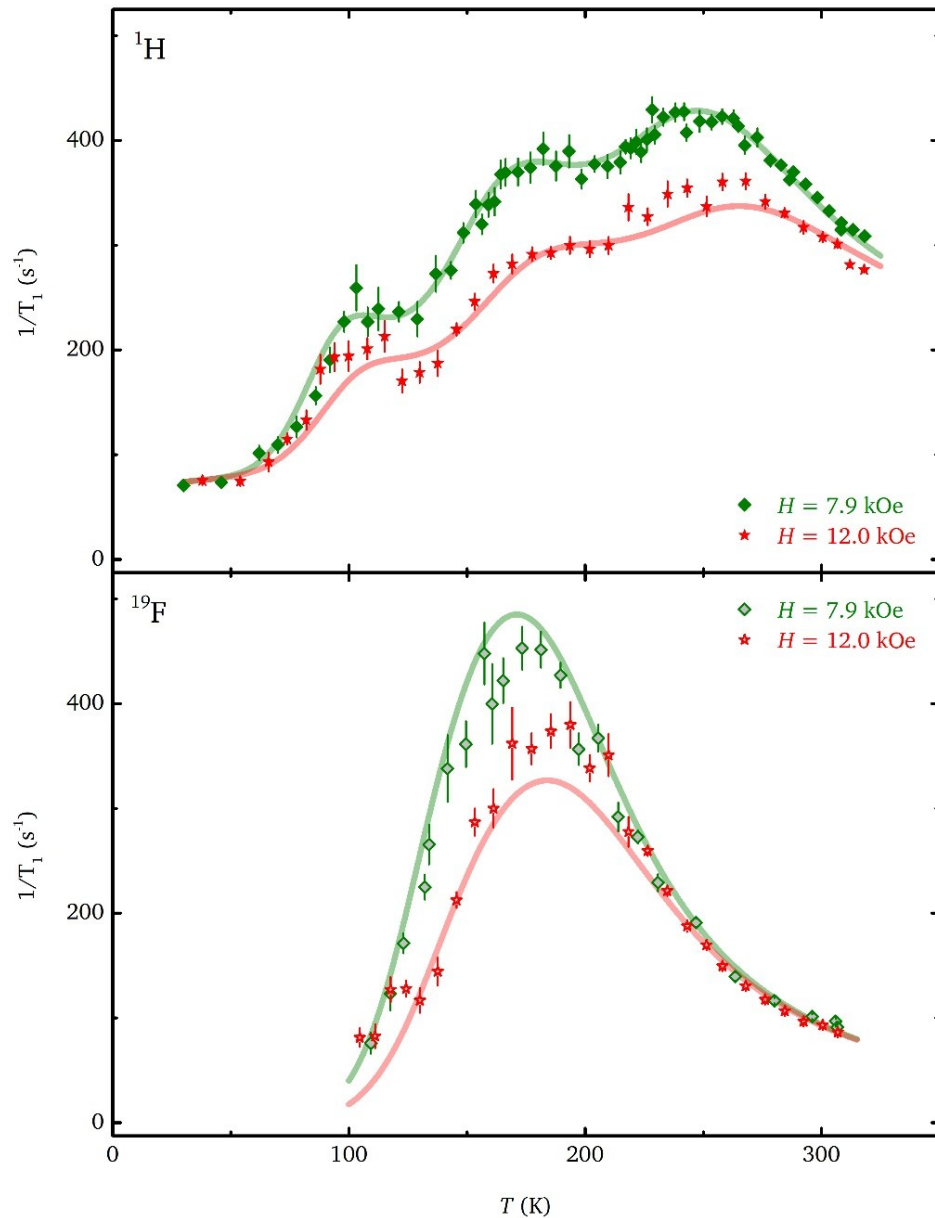
Signal clearly resolved for both nuclei.

Progressive inhomogeneous broadening induced by ferromagnetic phase.



$$\frac{1}{T_1} \propto \underbrace{\int_{-\infty}^{+\infty} d\tau \langle h_{\perp}(\tau) h_{\perp}(0) \rangle \exp(i\omega_L \tau)}_{J(\omega_L)}$$

Spin-lattice relaxation rate

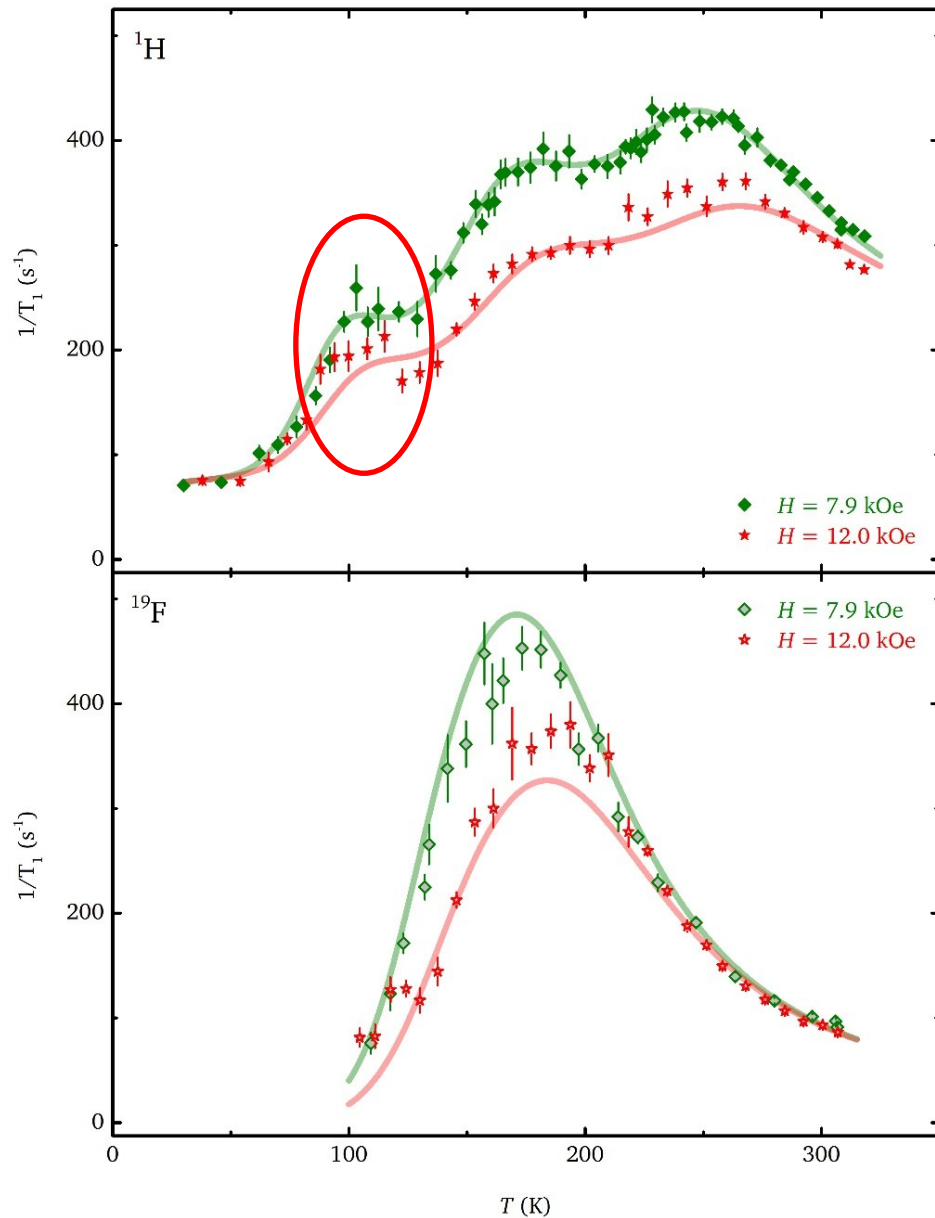


Weak bump at around 100 K
(^1H only).

Marked maximum at around 170 K
(both ^1H and ^{19}F).

Marked maximum at around 250 K
(^1H only).

Spin-lattice relaxation rate

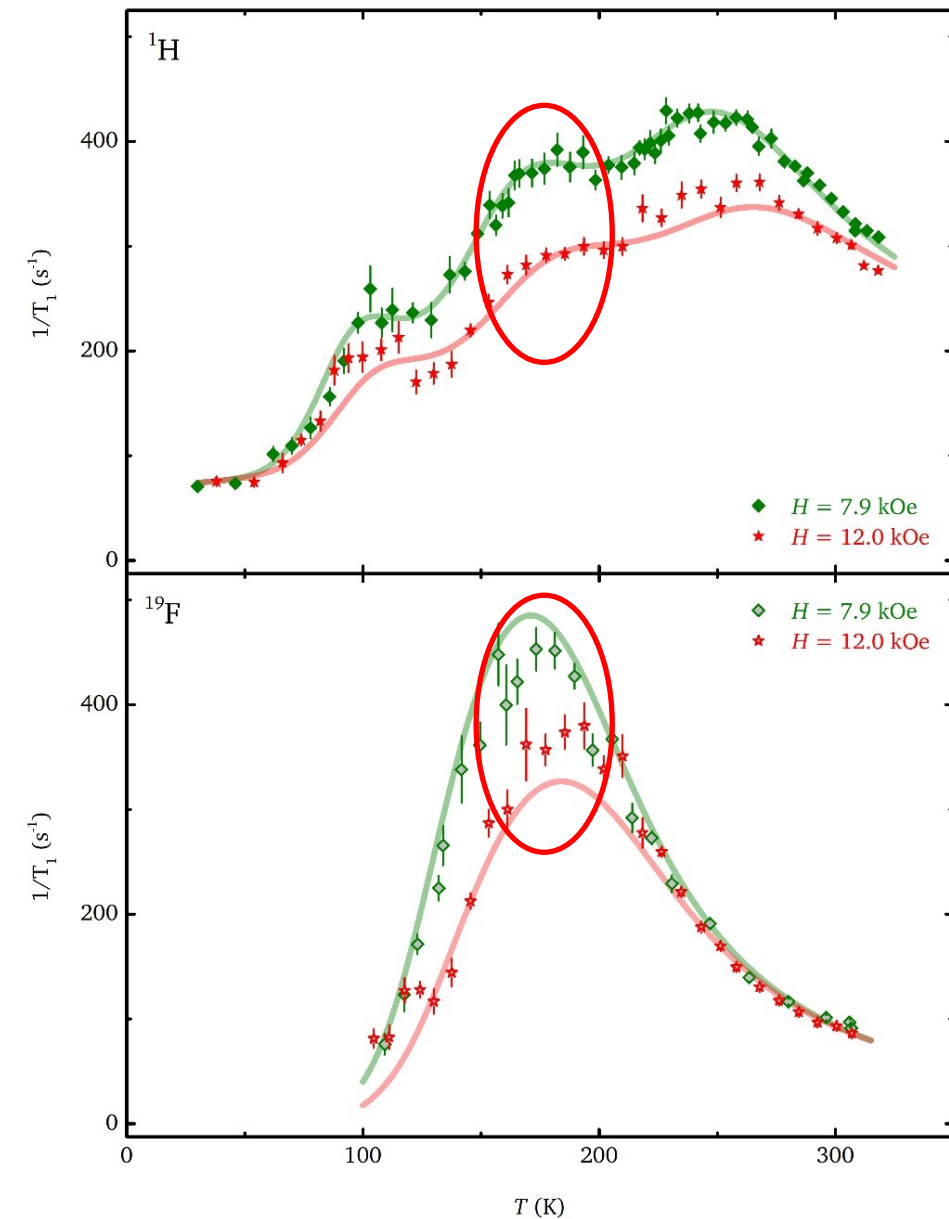


Weak bump at around 100 K
(^1H only).

Marked maximum at around 170 K
(both ^1H and ^{19}F).

Marked maximum at around 250 K
(^1H only).

Spin-lattice relaxation rate

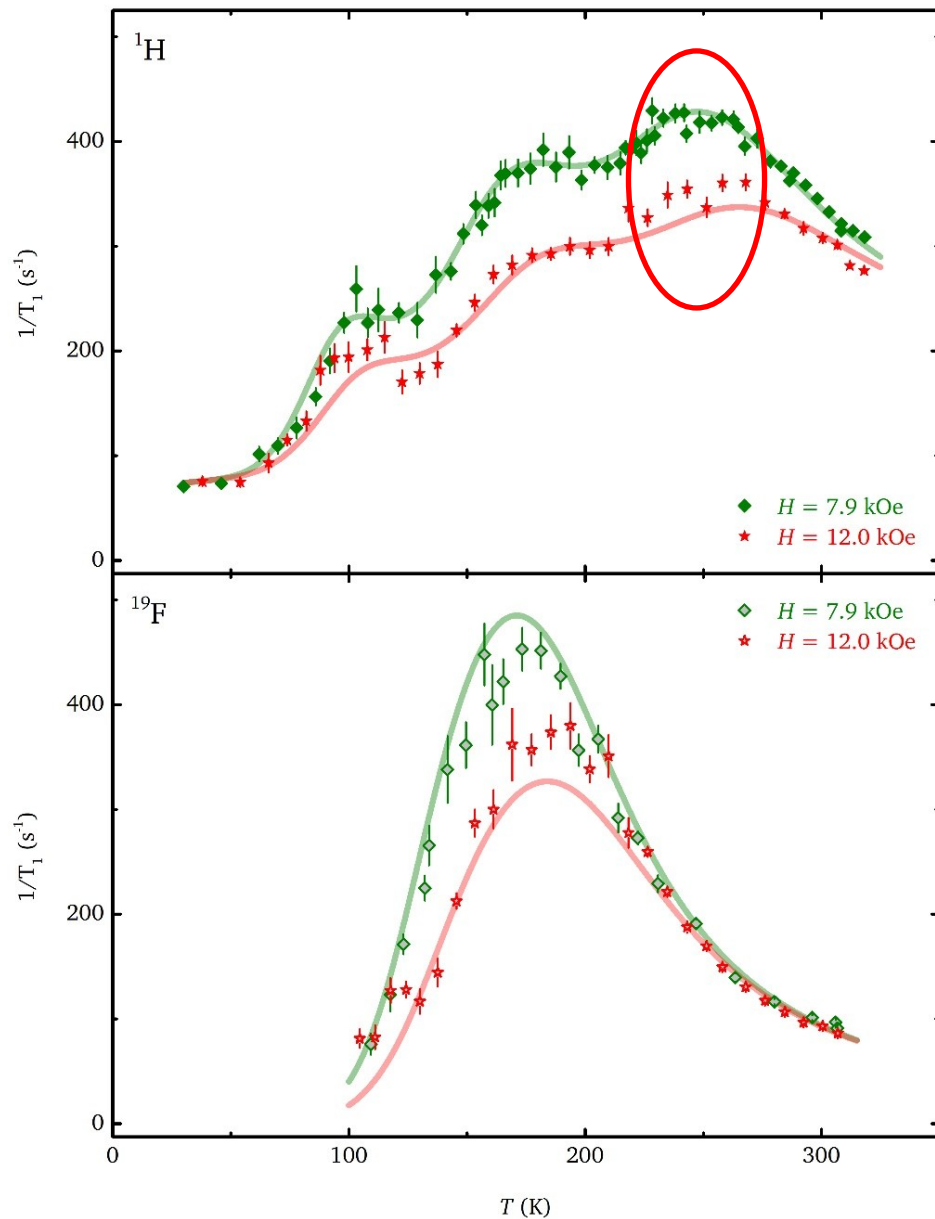


Weak bump at around 100 K
(1H only).

Marked maximum at around 170 K
(both 1H and ^{19}F).

Marked maximum at around 250 K
(1H only).

Spin-lattice relaxation rate



Weak bump at around 100 K
(^1H only).

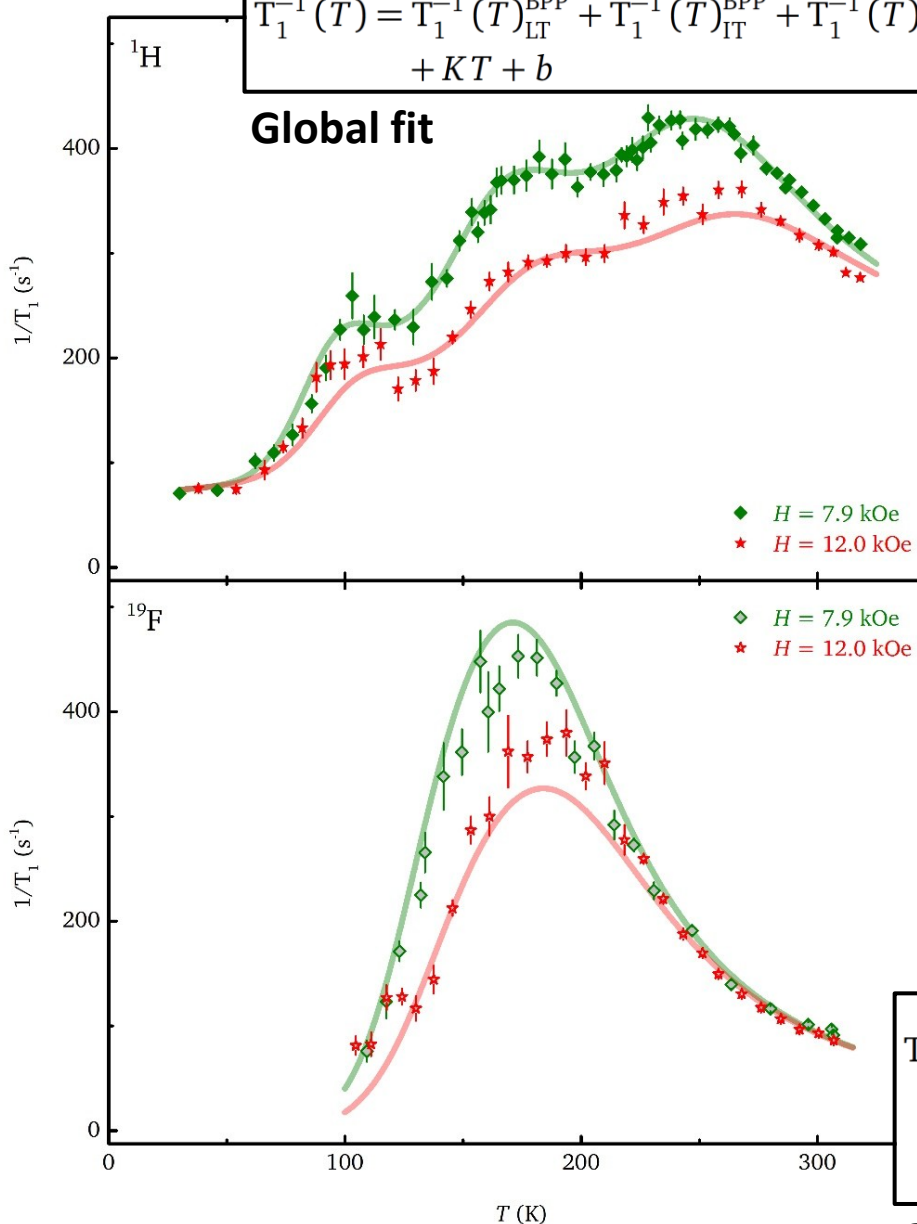
Marked maximum at around 170 K
(both ^1H and ^{19}F).

Marked maximum at around 250 K
(^1H only).

Spin-lattice relaxation rate

$$T_1^{-1}(T) = T_1^{-1}(T)_{\text{LT}}^{\text{BPP}} + T_1^{-1}(T)_{\text{IT}}^{\text{BPP}} + T_1^{-1}(T)_{\text{HT}}^{\text{BPP}} + KT + b$$

Global fit



Weak bump at around 100 K
(^1H only).

Marked maximum at around 170 K
(both ^1H and ^{19}F).

Marked maximum at around 250 K
(^1H only).

$$T_1^{-1}(T)^{\text{BPP}} = CJ(\omega_L)$$

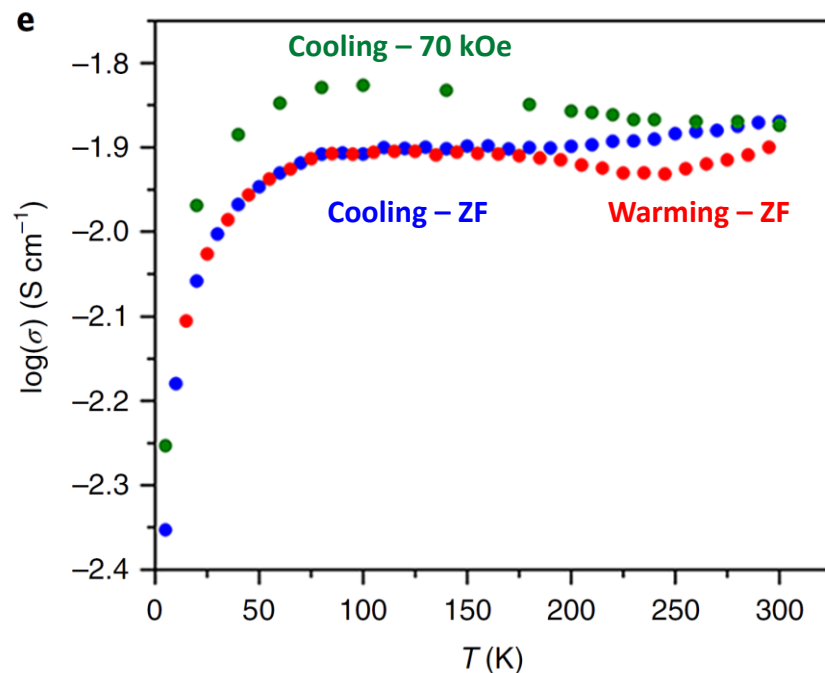
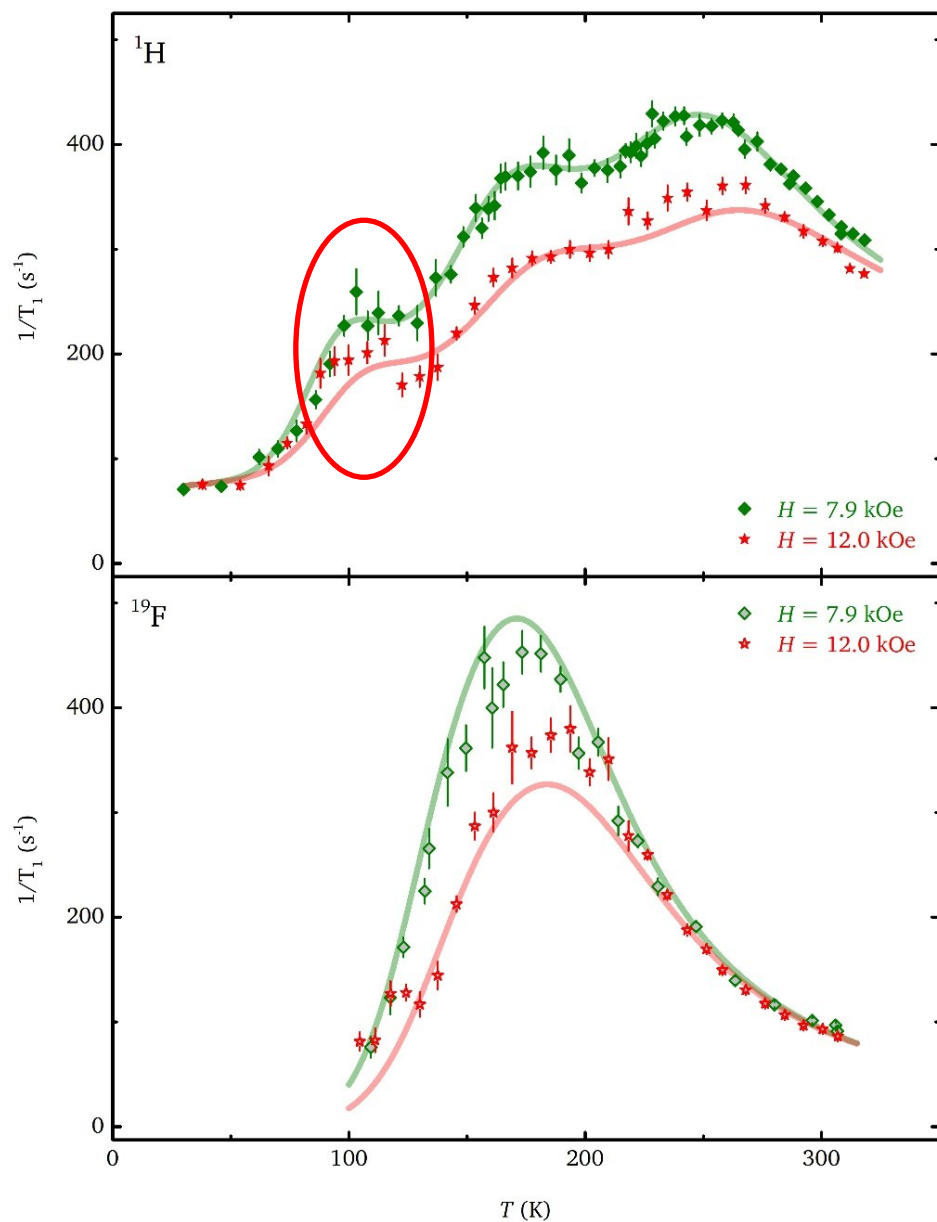
$$J(\omega) = \frac{\tau_c}{1 + \omega^2 \tau_c^2} \quad C \sim \gamma^2 \langle \Delta B^2 \rangle$$

$$\tau_c = \tau_0 \exp(\vartheta/T)$$

$$T_1^{-1}(T) = \frac{C T}{4\omega_L \delta \vartheta} \left\{ \arctan \left[\sinh \left(\frac{\vartheta + \delta \vartheta}{T} + \ln(\omega_L \tau_0) \right) \right] - \arctan \left[\sinh \left(\frac{\vartheta - \delta \vartheta}{T} + \ln(\omega_L \tau_0) \right) \right] \right\}$$

Global fit

Low temperatures

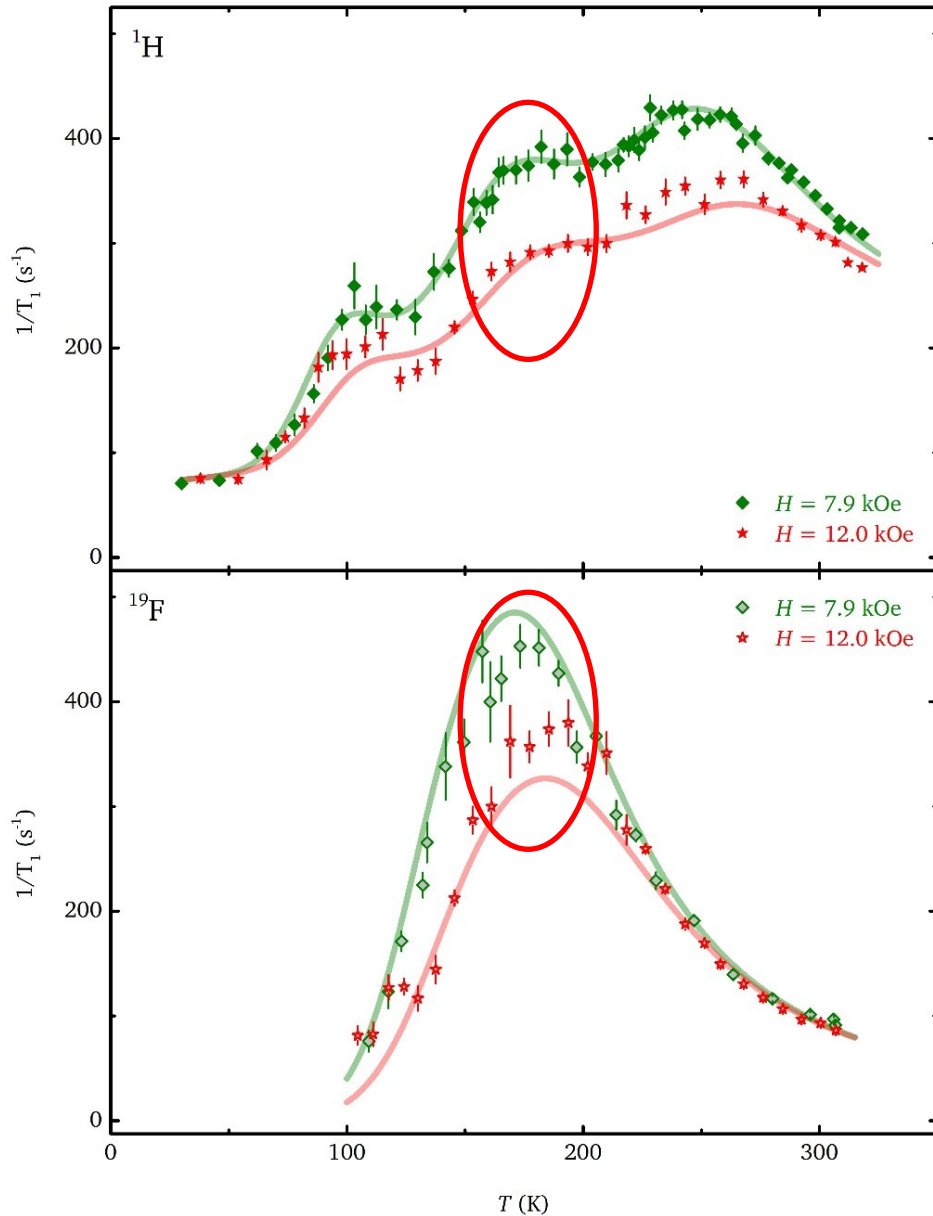


Correlation with sudden decrease of electrical conductivity.

Likely impact of charge localization probed by ^1H nuclei in the MOF structure.

Weak signal amplitude hampers further investigation of this region.

Intermediate temperatures



$$T_1^{-1}(T) = T_1^{-1}(T)_{\text{LT}}^{\text{BPP}} + T_1^{-1}(T)_{\text{IT}}^{\text{BPP}} + T_1^{-1}(T)_{\text{HT}}^{\text{BPP}} + KT + b$$

	C (10^{10} s^{-2})	τ_0 (10^{-11} s)	ϑ (K)
LT	5.65 ± 0.25	3.4 ± 1.7	500 ± 50
IT	9.0 ± 0.5	1.8 ± 0.6	960 ± 60
HT	9.4 ± 0.4	1.20 ± 0.15	1525 ± 35

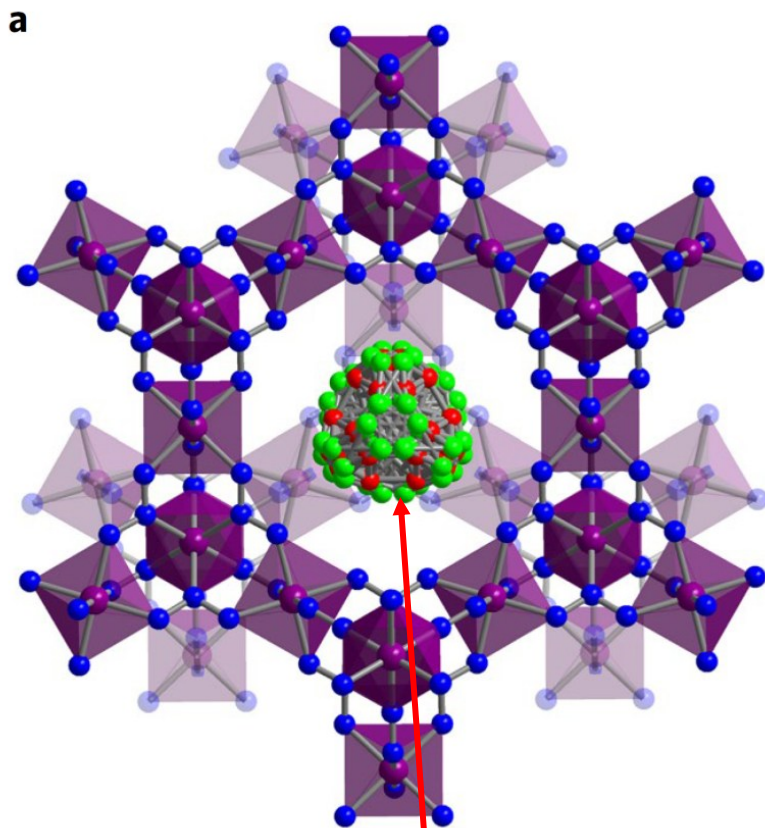
$$T_1^{-1}(T) = \frac{C T}{4\omega_L \delta\vartheta} \left\{ \arctan \left[\sinh \left(\frac{\vartheta + \delta\vartheta}{T} + \ln(\omega_L \tau_0) \right) \right] - \arctan \left[\sinh \left(\frac{\vartheta - \delta\vartheta}{T} + \ln(\omega_L \tau_0) \right) \right] \right\}$$

C (10^{11} s^{-2})	τ_0 (10^{-11} s)	ϑ (K)	$\delta\vartheta$ (K)
2.35 ± 0.05	1.4 ± 0.1	990 ± 15	205 ± 15

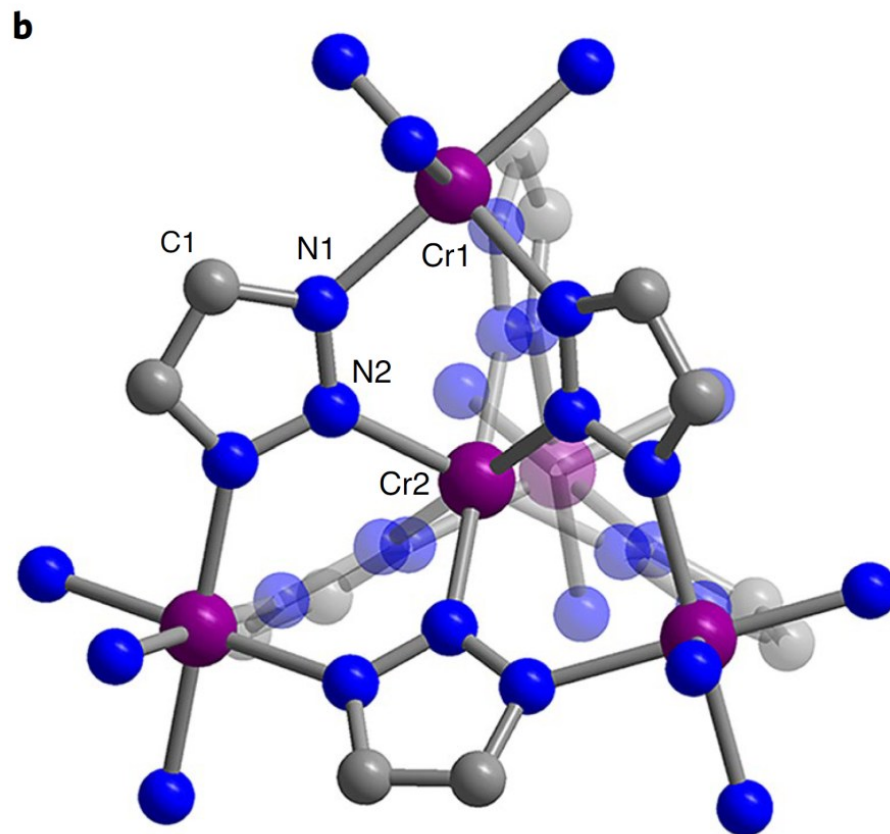
Both nuclei probe the same dynamics.

Intermediate temperatures

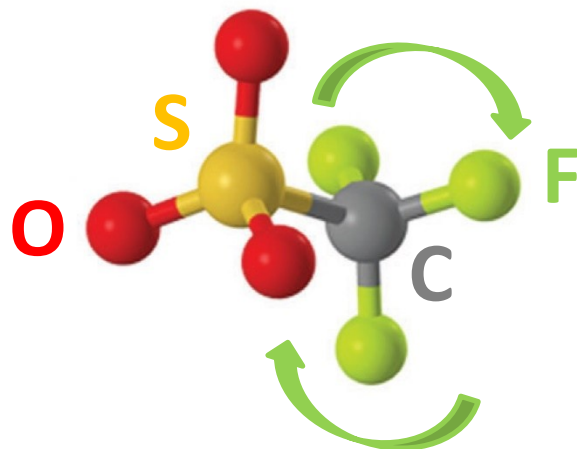
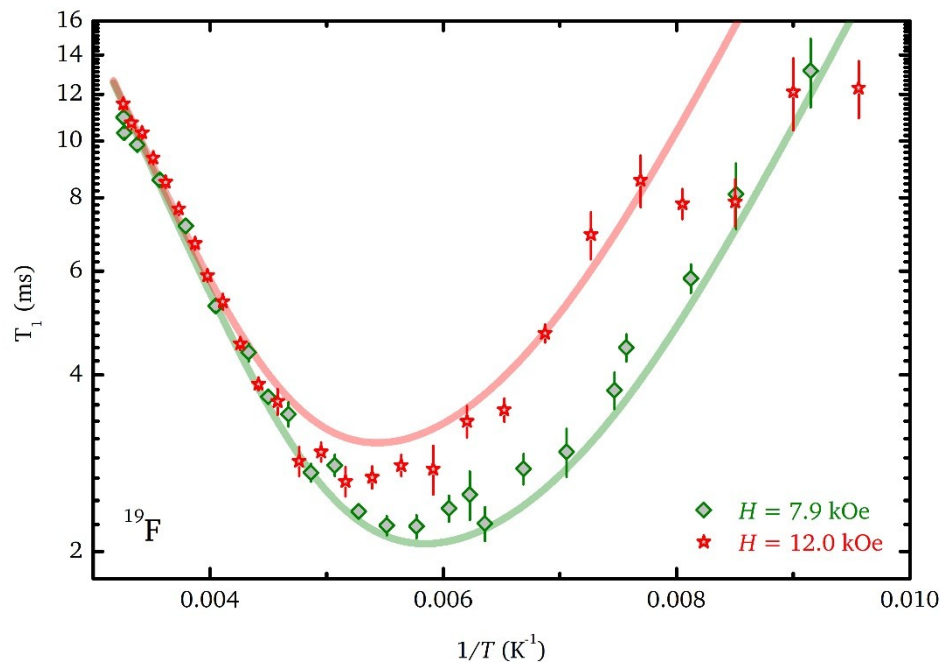
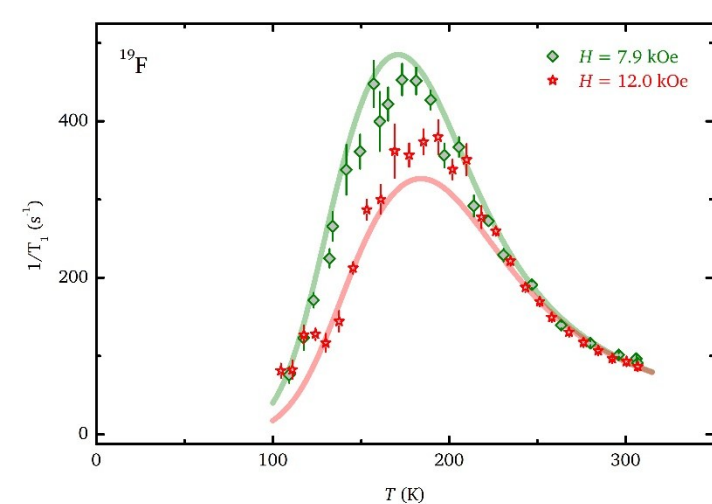
^1H nuclei in the metal-organic framework.



^{19}F nuclei in the charge-balancing triflate anion.



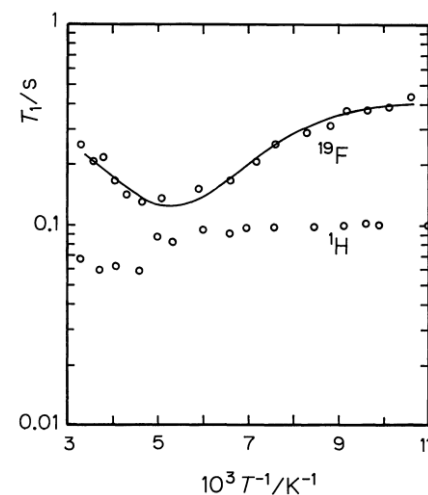
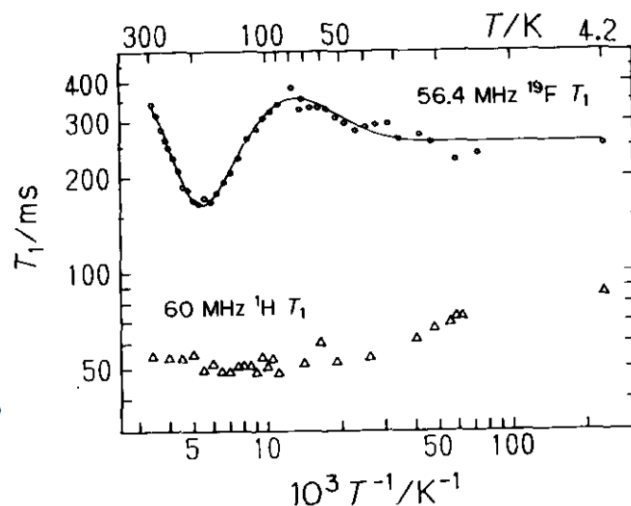
Intermediate temperatures



$$\vartheta = 900 \div 1300 \text{ K}$$

$$C \sim \gamma^2 \langle \Delta B^2 \rangle$$

$$\tau_0 = 10^{-12} \div 10^{-11} \text{ s}$$

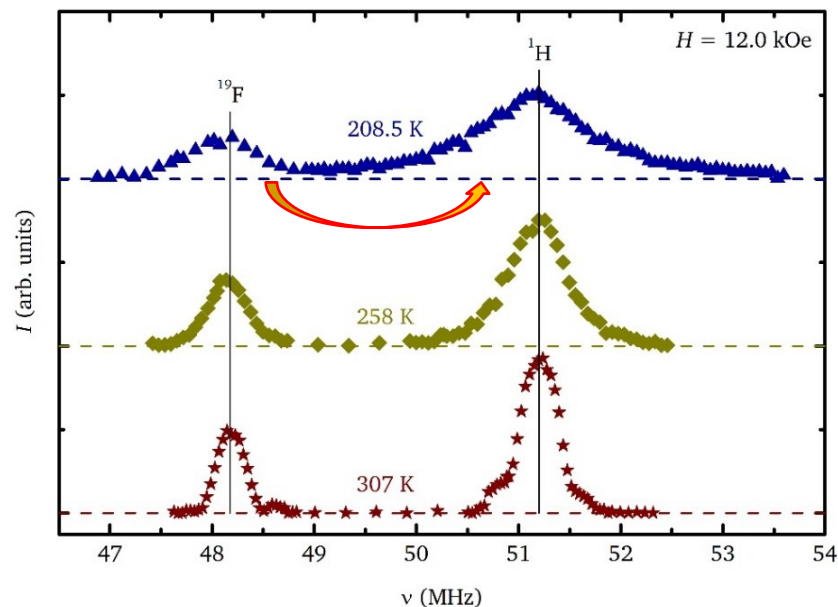
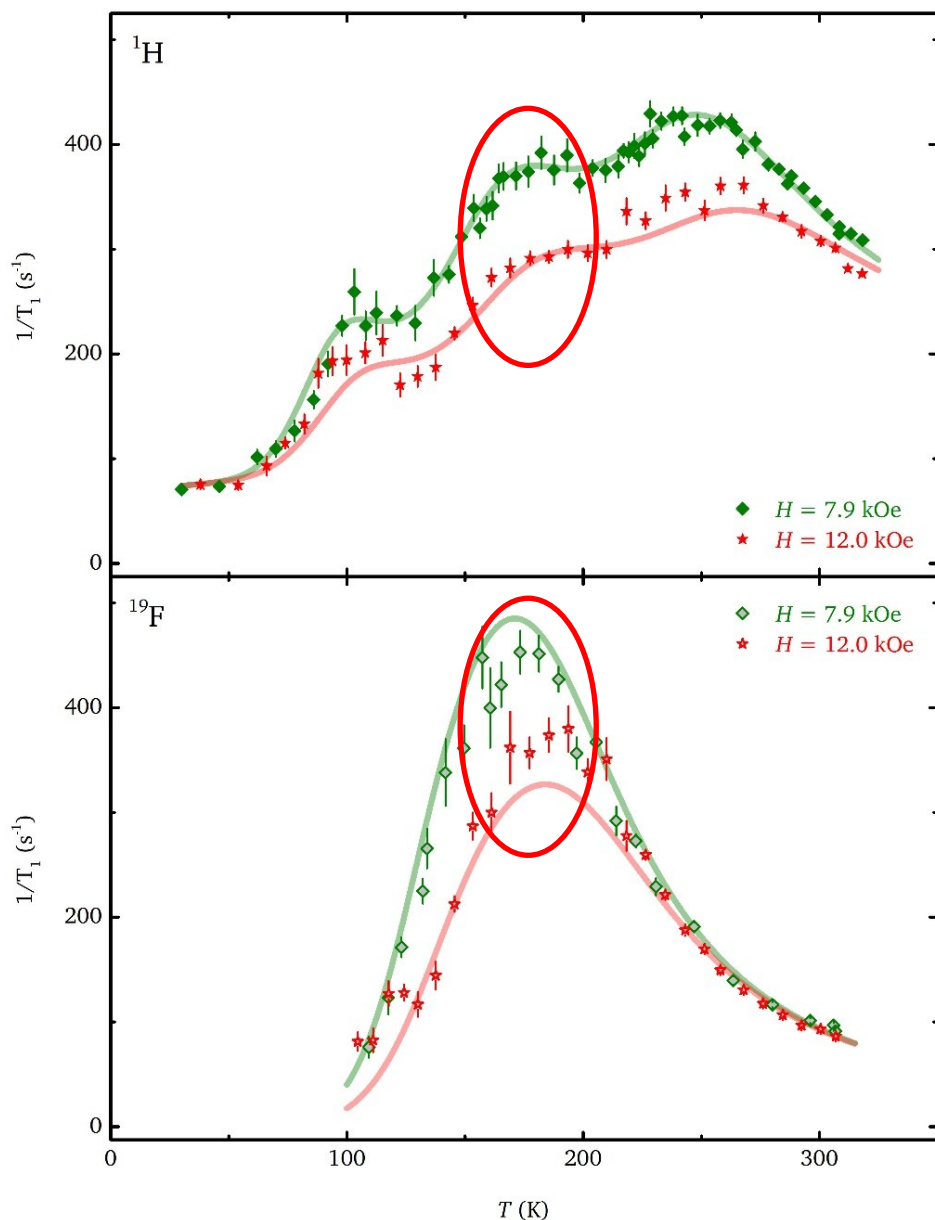


Intense fluctuating field in MOF (around 10 times). Rotary dynamics in FM background.

Intermediate temperatures

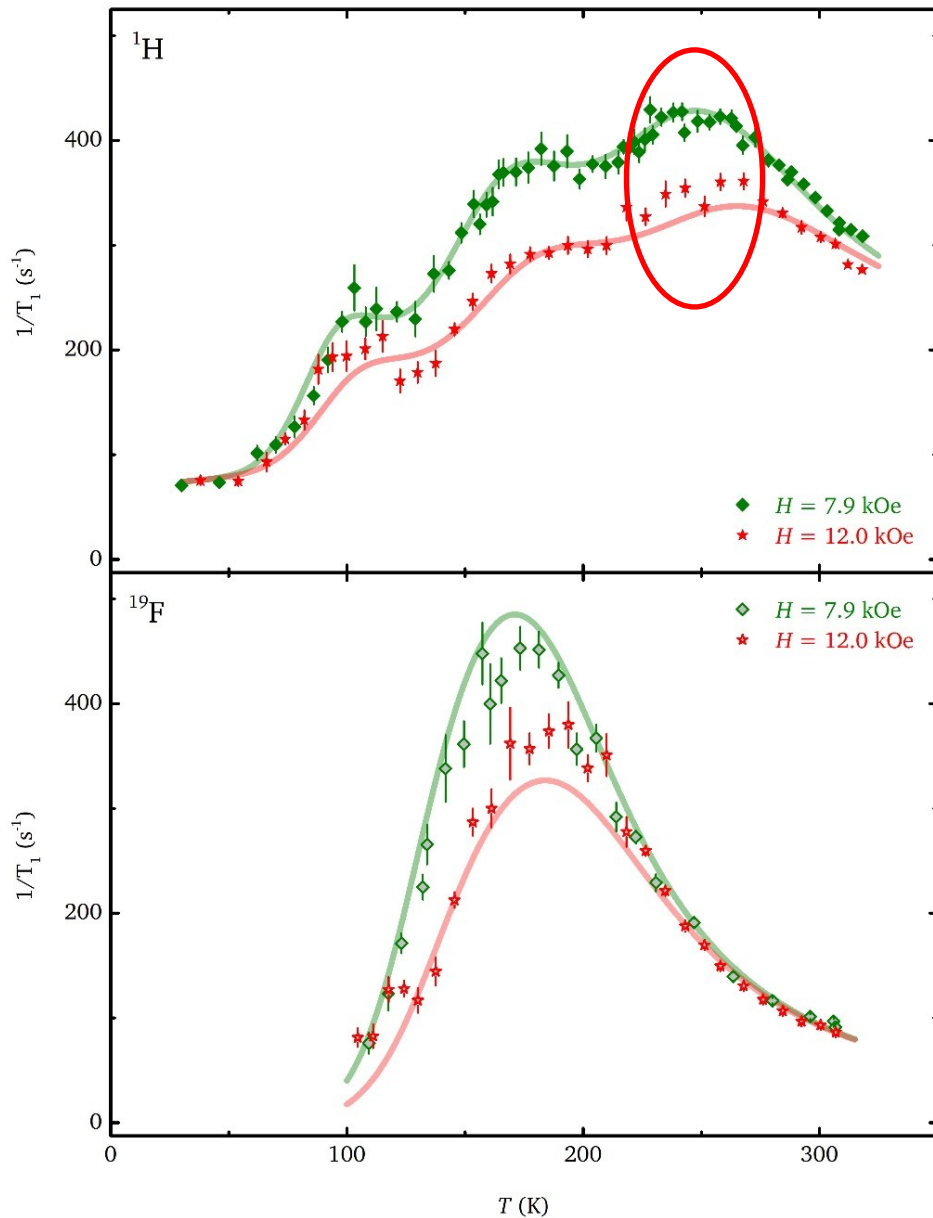
Molecular rotary dynamics induces relaxation at intermediate temperatures.

Short relaxation times on ^{19}F : intense local fluctuating magnetic fields due to the ferromagnetic background.



Cross-relaxation on ^1H induced by spin diffusion over the broadened line.

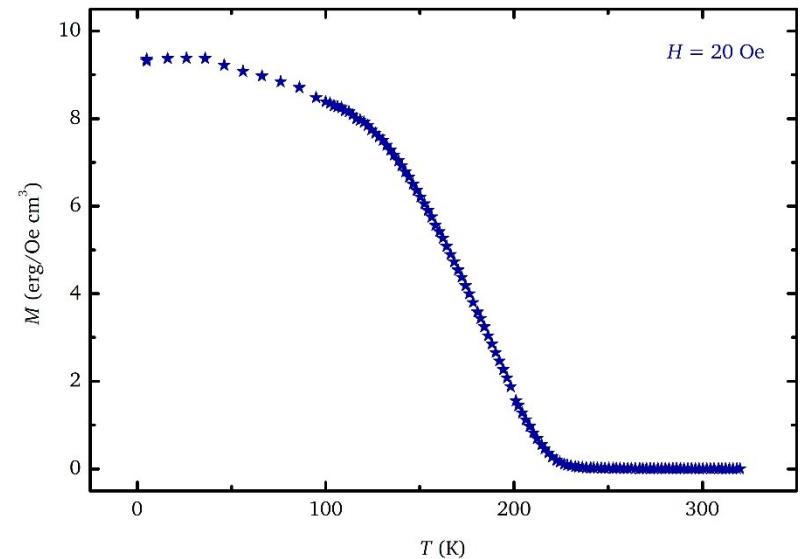
High temperatures



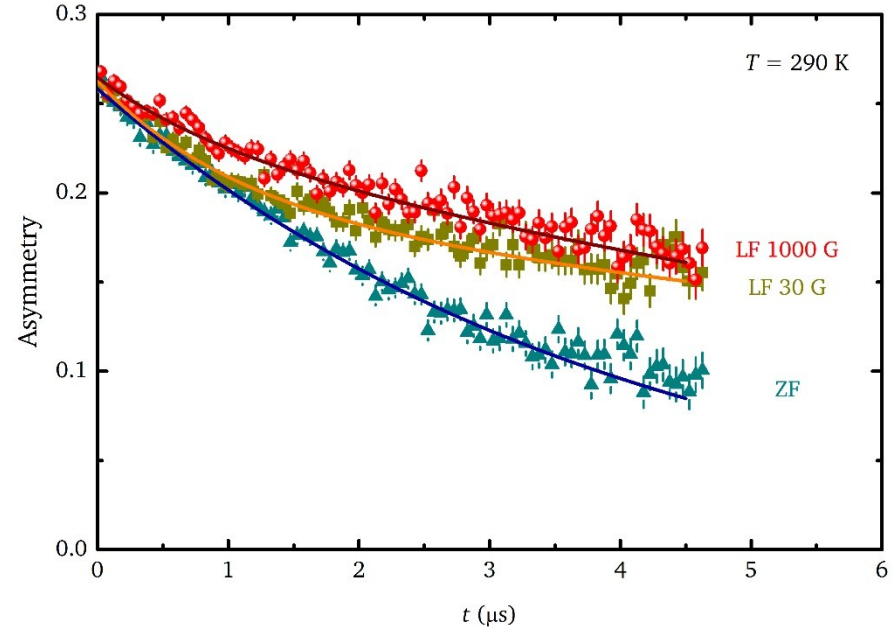
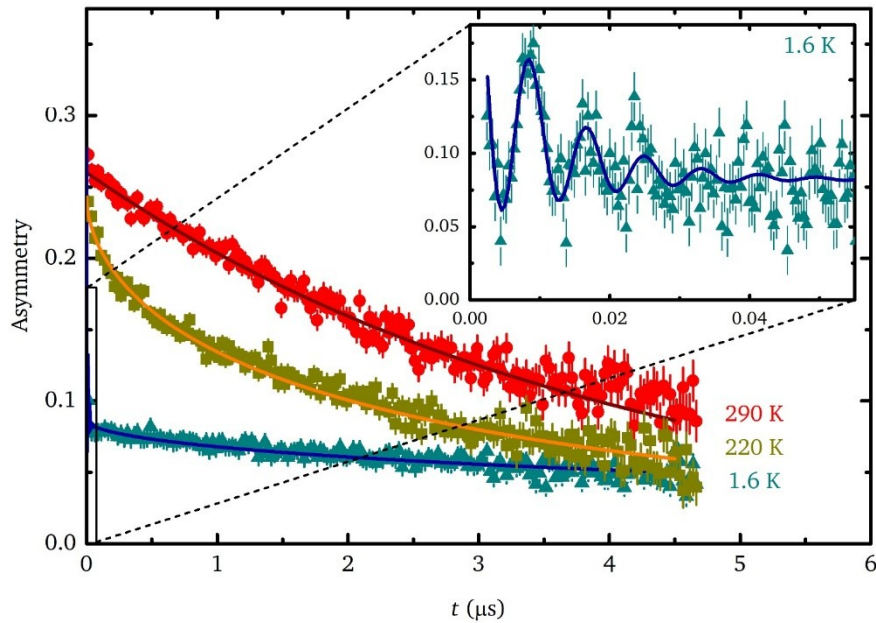
Lack of any sharp anomaly due to critical dynamics at the critical temperature.

Persistence of slow, activated dynamics probed by ^1H on the MOF.

Unconventional nature of the paramagnetic/ferromagnetic transition.



High temperatures



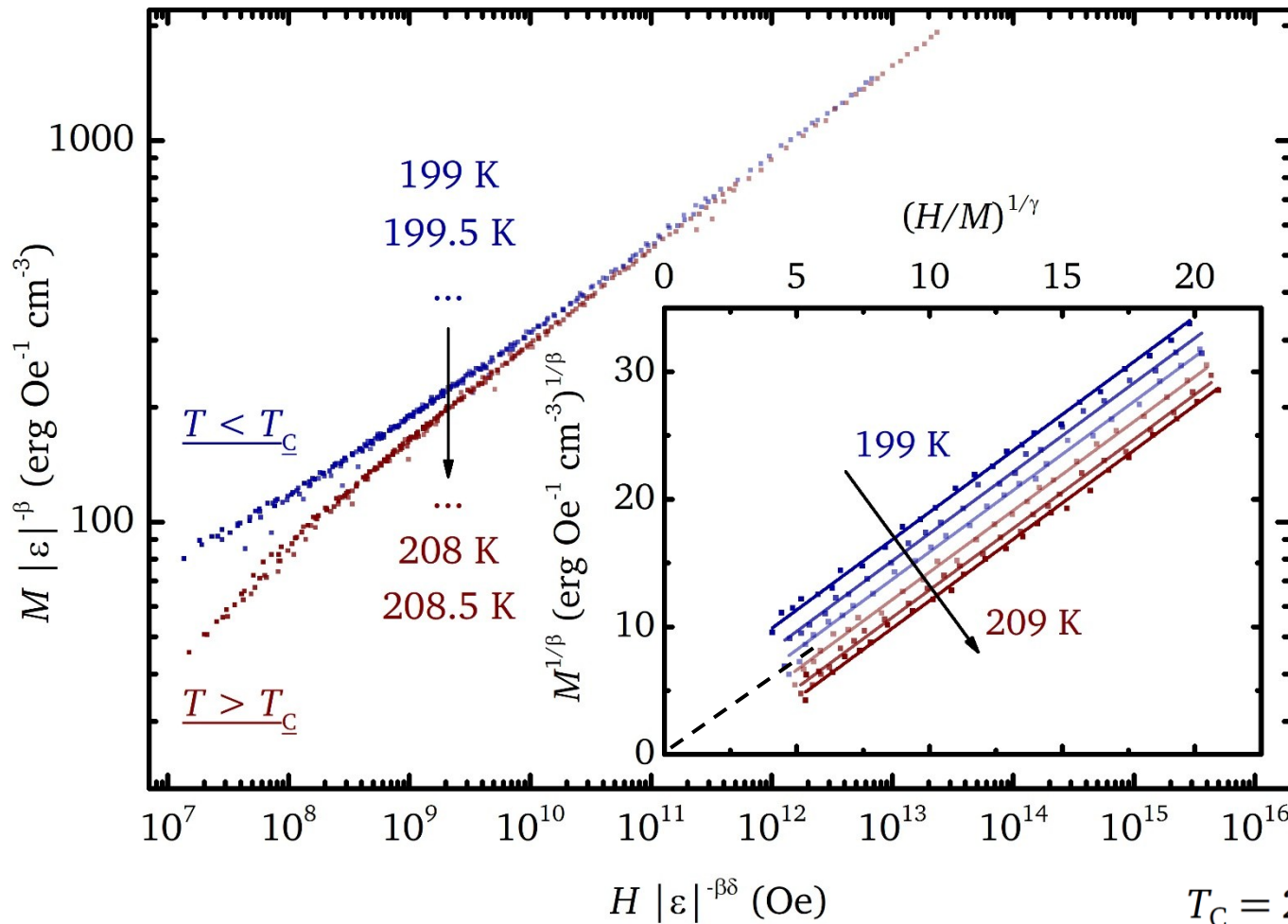
$$\frac{A(t)}{A(0)} = a_{T_1} \cos(\gamma_\mu B_\mu t + \phi) \exp(-\lambda_{T_1} t) + a_{T_2} \exp(-\lambda_{T_2} t) + a_L \exp(-\lambda_L t)$$

Likely implantation site close to Cr ions.

Low-temperatures Bloch-like $T^{3/2}$ law (FM).

Unusual survival of dynamics well-above the critical temperature.

High temperatures



$$H = H_{ext} - 4\pi N M$$

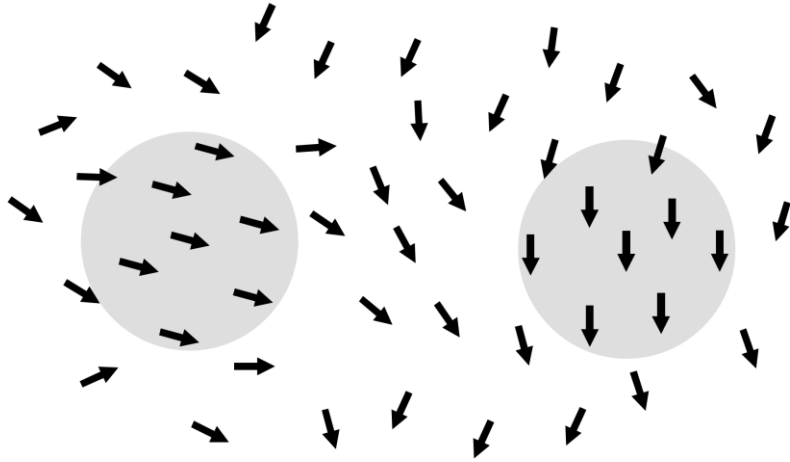
$$\frac{M}{|\varepsilon|^\beta} = F_\pm \left(\frac{H}{|\varepsilon|^{\beta\delta}} \right)$$

$$\varepsilon = \frac{T - T_c}{T_c}$$

Isothermal dc magnetometry
- Static scaling
- Arrott-Noakes approach

	Results	3D Heisenberg	Mean-field
β	0.73	0.36	0.5
δ	4.2	4.86	3
γ	2.336	1.39	1

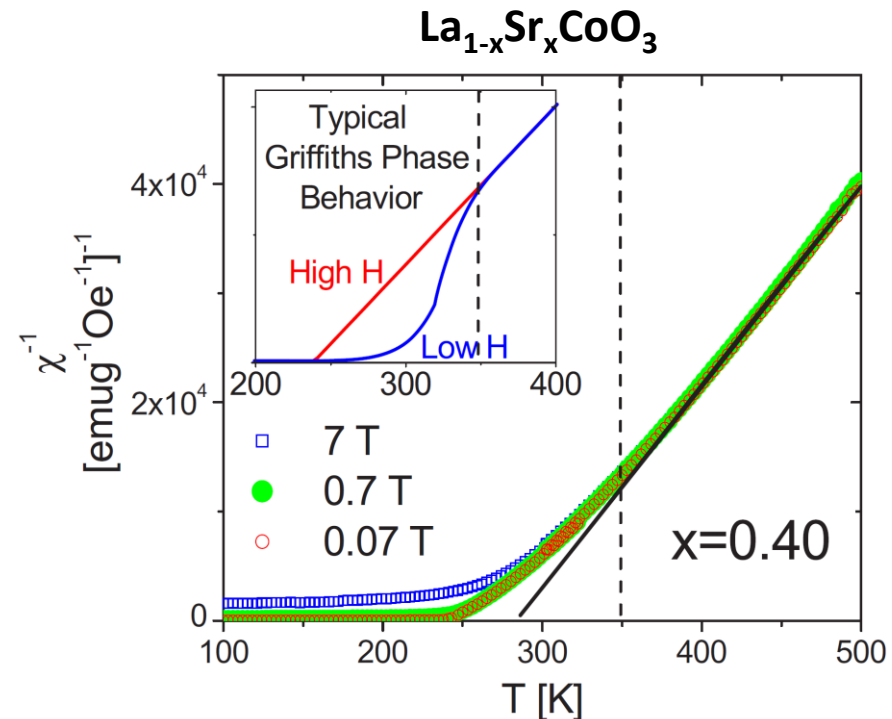
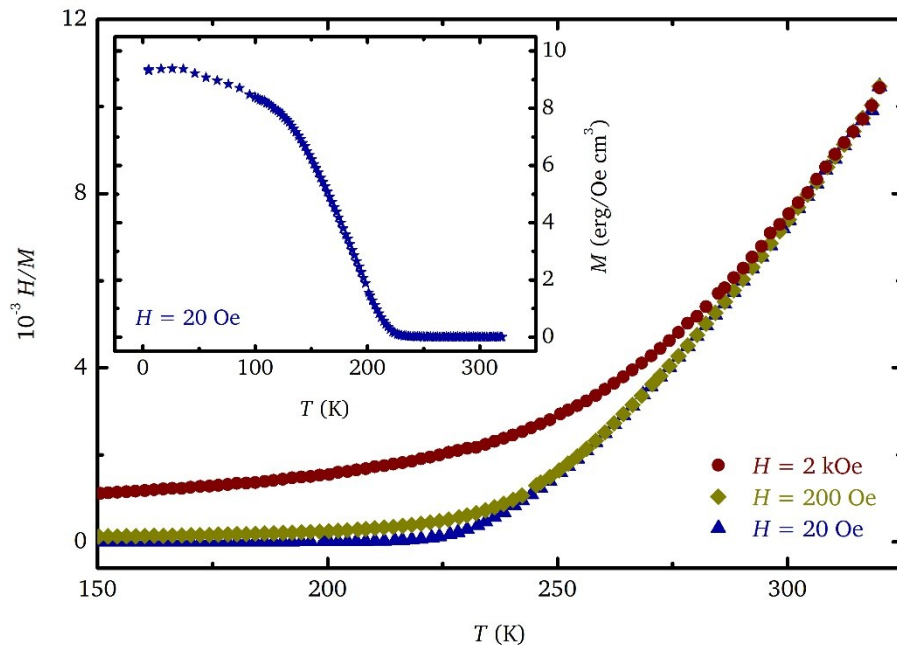
Clustered state



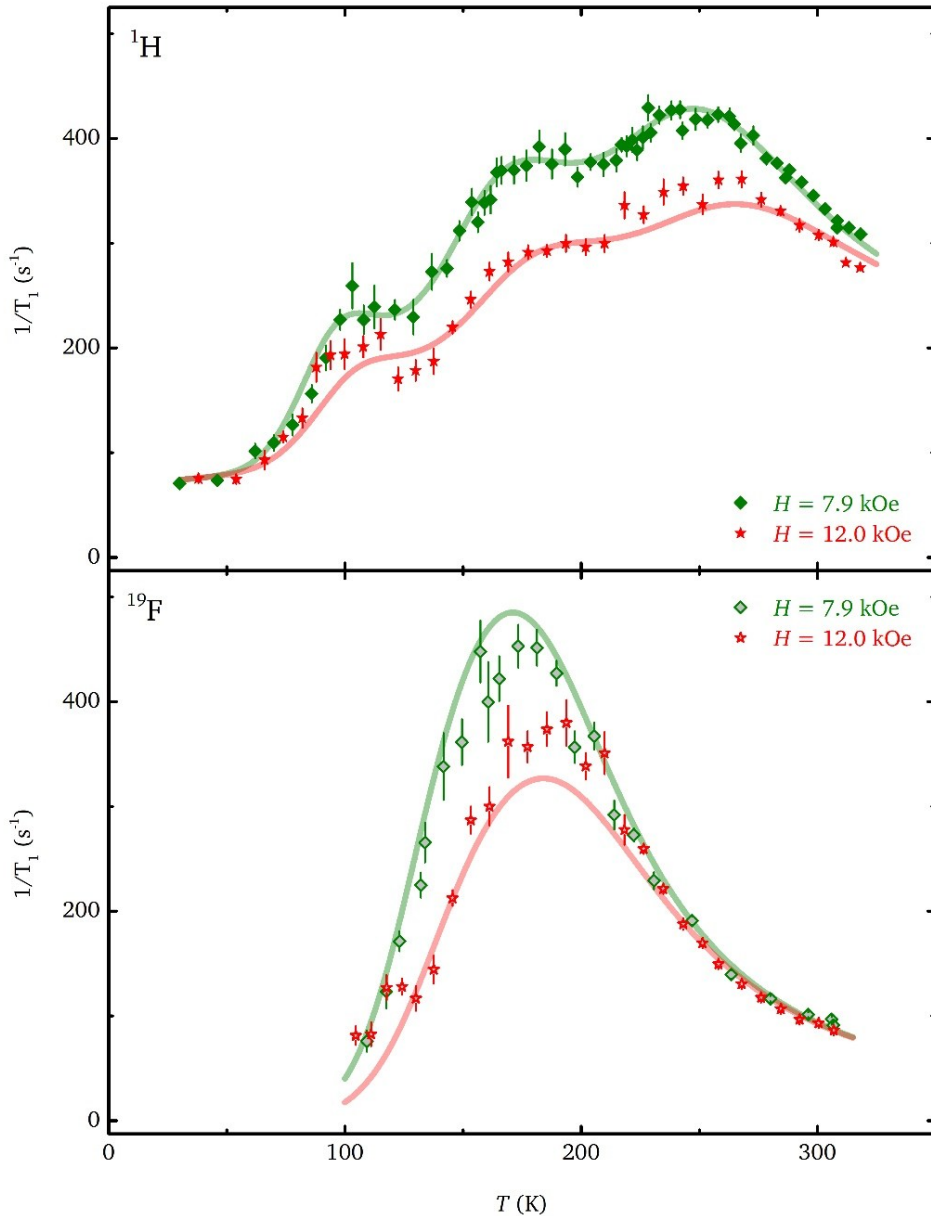
Unusual values of critical exponents compatible with magnetoelectronic phase separation above T_c (manganites, cobaltites).

Magnetization not compatible with development of clustered Griffiths state.

Persisting slow dynamics due to clusters.



Summary



Low temperatures:

evidences of charge localization from electrical conductivity suggests the origin of the NMR relaxation.

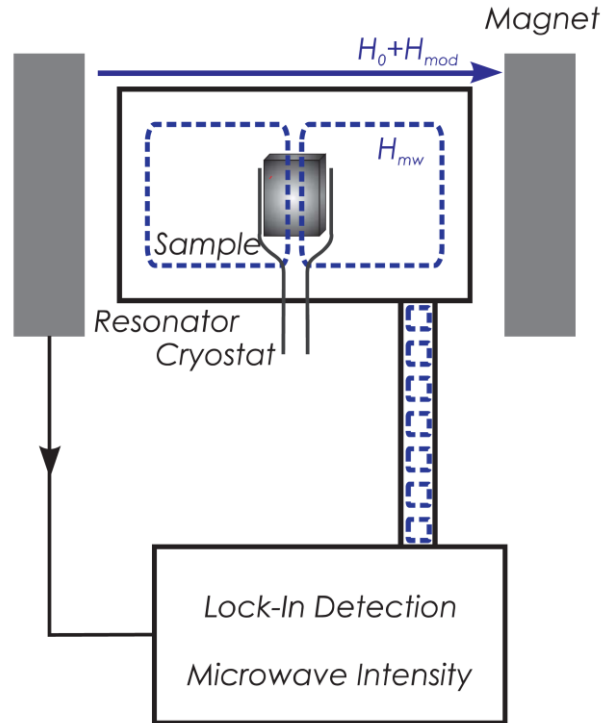
Intermediate temperatures:

rotary dynamics of triflate anion in a FM background drives relaxation on ¹⁹F and on ¹H in turn.

High temperatures:

unusual persistence of slow dynamics tracked by NMR and muon-spin rotation. Likely origin in magnetoelectronic phase separation in the paramagnetic phase, resembling what observed in oxides.

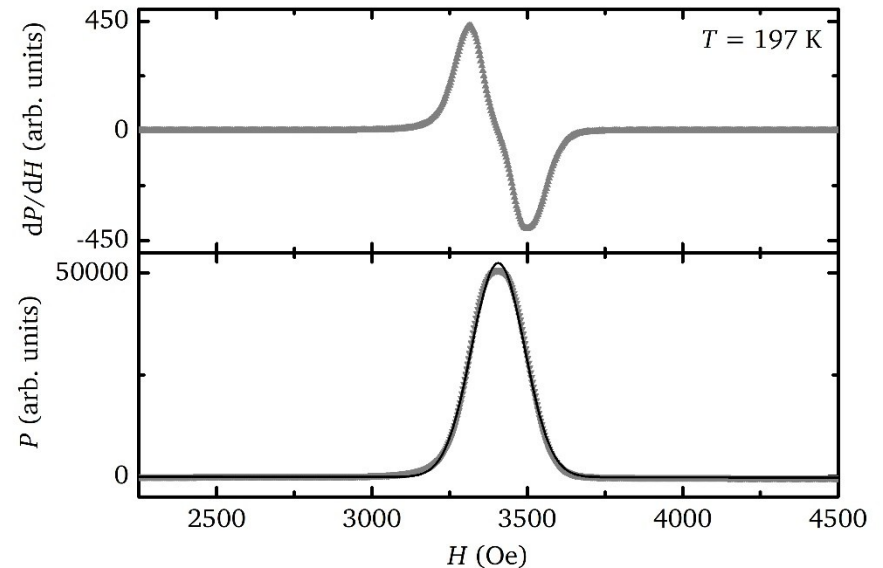
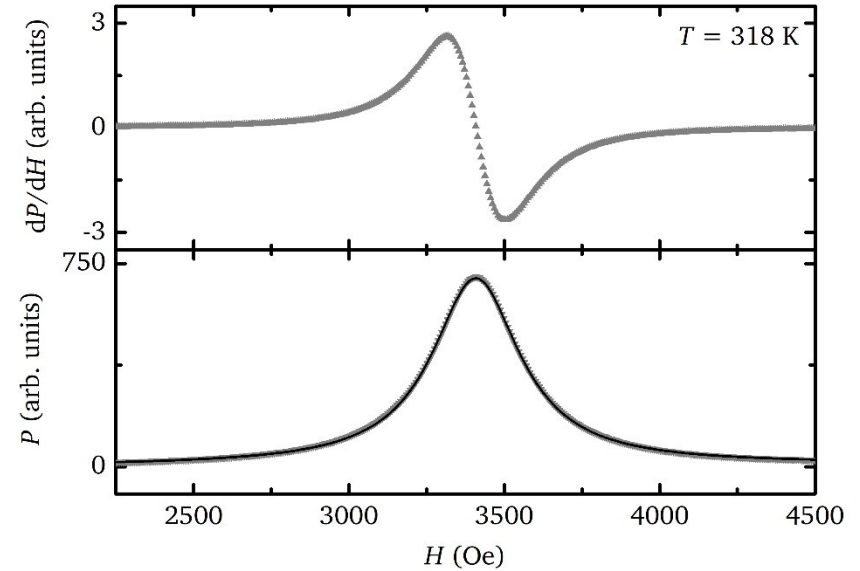
Ferromagnetic resonance (X-band)



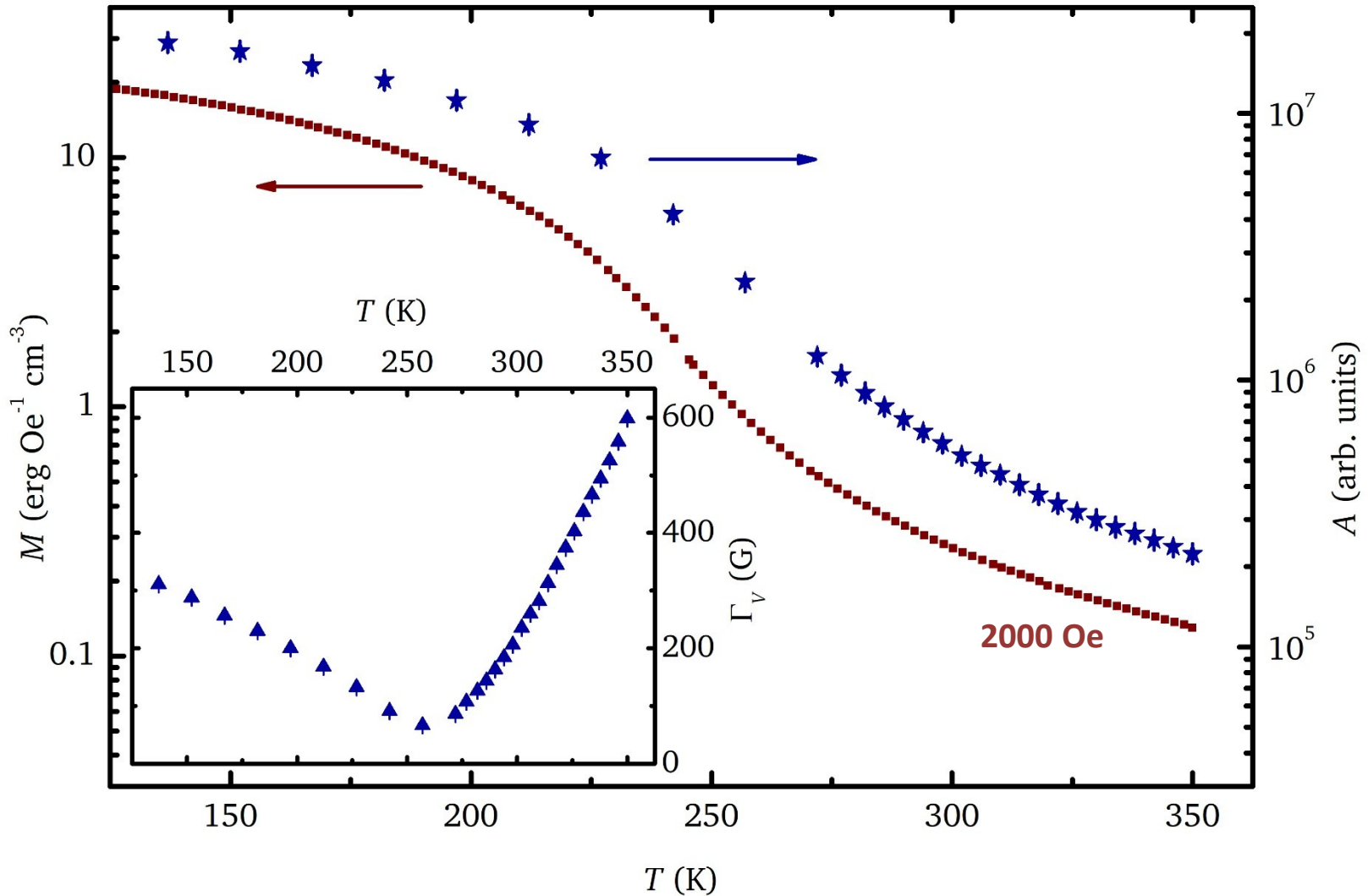
Voigt lineshape:

$$y = \frac{2A}{\Gamma_G} \left(\frac{\ln(2)}{\pi} \right)^{1/2} \frac{a}{\pi} \int_{-\infty}^{+\infty} \frac{\exp(-t^2)}{a^2 + (\nu - t)^2} dt + B \cdot H + y_0$$

$$a = \sqrt{\ln(2)} \frac{\Gamma_L}{\Gamma_G} \quad \Gamma_V \simeq 0.5346 \Gamma_L + \sqrt{0.2166 \Gamma_L^2 + \Gamma_G^2}$$



Ferromagnetic resonance (X-band)



Conventional correlation between FMR amplitude and dc magnetization + conventional behaviour of lineshape.

No anomaly detected around 170 K. Nuclear relaxation not of magnetic origin at intermediate temperatures.